International Journal of Earth Sciences
https://doi.org/10.1007/s00531-024-02476-w

ORIGINAL PAPER

Contact metamorphism and dolomitization overprint on Cambrian carbonates from the Ossa-Morena Zone (SW Iberian Massif): implications to Sr-chronology of carbonate rocks

José Roseiro[1,2,3] · Noel Moreira[1,2,3] · Laura Andrade[1] · Pedro Nogueira[1,2] · Daniel de Oliveira[4,5] · Luis Eguiluz[6] · José Mirão[1,7] · Patrícia Moita[1,7] · José Francisco Santos[8] · Sara Ribeiro[8] · Jorge Pedro[1,2]

Received: 24 June 2024 / Accepted: 16 October 2024

Abstract

The Cambrian Series 2 Carbonate Formation from the Alter do Chão Elvas-Cumbres Mayores unit (Ossa-Morena Zone, SW Iberian Massif) is composed of regionally metamorphosed marbles and marlstones that underwent chlorite zone metamorphism and preserve the primaeval limestone $^{87}Sr/^{86}Sr$ ratios (0.7083–0.7088). These are consistent with the established Lower Cambrian seawater curve, and therefore used for age constraints in formations lacking fossil contents. The regional mineralogical and Sr-isotopic features of the carbonate rocks are frequently overprinted by the effects of contact metamorphism induced by magmatic bodies emplaced during rift-related and synorogenic events of the Palaeozoic, as well as by post-metamorphic dolomitization processes. The development of calc-silicate minerals due to contact metamorphism is common in the rocks of the Carbonate Formation and apparently results from the interaction of the protolith with fluids of different origin: (i) internally produced fluids released by conductive heating (observed in external contact aureoles) and (ii) external intrusion-expelled fluids that, besides leading to the appearance of distinctive assemblages, also promote an influx of strontium content (observed in roof pendants). Calc-silicate mineralogy varies substantially throughout the region, likely due to the heterogeneous distribution of silicate minerals of the protolith, progression of intrusion-driven fluids, and the irregular effect of thermal gradients. Results suggest that high-grade contact metamorphism (hornblende facies or higher) and dolomitization processes imposed on the Carbonate Formation significantly influence the isotopic signatures of the carbonates, providing limitations in applying Sr-isotopic chronology.

Keywords $^{87}Sr/^{86}Sr$ isotopes · Marbles · Calc-silicate mineralogy · Contact metamorphism · Dolomitization · Ossa-Morena Zone

✉ José Roseiro
jdbwr@uevora.pt

1 Dpt. Geociências, Escola de Ciências e Tecnologias da Universidade de Évora, Rua Romão Ramalho 59, 7000-761 Évora, Portugal

2 Instituto de Ciências da Terra (ICT), Polo de Évora, Rua Romão Ramalho 59, 7000-761 Évora, Portugal

3 Instituto de Investigação e Formação Avançada, Universidade de Évora, Palácio Do Vimioso, Largo Marquês de Marialva Apt 94, 7002-554 Évora, Portugal

4 Laboratório Nacional de Energia e Geologia, Mineral Resources and Geophysics Research Unit, Estrada da Portela, Bairro Do Zambujal Apt 7586, Alfragide, 2610-999 Amadora, Portugal

5 Mineral Resources Expert Group, EuroGeoSurveys, Rue Joseph II 36-38, Box 7, 1000 Brussels, Belgium

6 Dpt. Geodinámica, Facultad de Farmacia, Universidad del País Vasco UPV/EHU, 01006 Vitoria, Spain

7 Laboratório HERCULES, Universidade de Évora, Palácio Do Vimioso, Largo Marquês de Marialva Apt 94, 7000-089 Évoravora, Portugal

8 GeoBioTec, Dpt Geociências, Lab Geologia Isotópica, Universidade de Aveiro, 3810-193 Aveiro, Portugal

Published online: 06 November 2024

Introduction

The variety of features preserved in calc-silicate-bearing rocks that resulted from the metamorphic recrystallization of carbonate rocks (primarily limestones and dolostones) are ascribed to interactions with chemically active fluids under specific pressure and temperature conditions through time and space. Thermal metamorphic reactions on pure carbonate rocks, originally composed almost exclusively of calcite or dolomite consist mainly of recrystallization of these phases, promoting crystal growth in an equidimensional fabric. However, the presence of accessory minerals concomitant with decarbonization and input from external fluids leads to the formation of a wide range of new assemblages (e.g., Sharma and Sharma 2020; Winter 2014) resulting in calc-silicate lithotypes (i.e., rocks with mineralogy in which calcium silicates are dominant). Calc-silicate and carbonate–silicate rocks spatially associated with calcite and dolomite marbles have been largely documented as products of contact metamorphism of primary carbonate rocks located in the vicinity of intrusions, usually developing a radial zonation with an increase of recrystallization and metamorphic grade toward the igneous body in aureoles of varying widths. The contact metamorphic facies are well described for metasedimentary rocks of detrital origin: the hornfels-facies, low P/T series (e.g., Winter 2020). Despite the designation made for index minerals in detrital metasedimentary rocks, these terms are applied to other lithologies in contact aureoles such as carbonate rocks (e.g., Sharma and Sharma 2020). Prograde isograds include: (i) low–grade albite–epidote facies at ca. 300–400 °C, (ii) medium-grade hornblende facies at ca. 400–550 °C, (iii) high-grade pyroxene facies at ca. 550–700 °C, and (iv) very high grade sanidine facies at temperatures higher than 700 °C. In thermally metamorphosed carbonate rocks, from low- to high-grade the common mineral assemblages are calcite, dolomite, minor quartz and calc-silicate minerals, namely: talc, tremolite, and epidote at low-grade (albite–epidote facies), diopside and grossular at medium-grade (hornblende facies), and scapolite, vesuvianite, forsterite and wollastonite (pyroxene facies) at high-grade (e.g., Sharma and Sharma 2020).

The presence of rocks bearing calc-silicate mineral assemblages is very common in long-lived carbonate basins that experienced magmatic events and regional metamorphism, providing good indicators of the tectono-magmatic and metamorphic evolution of key sectors in orogens. Good examples of such cases can be found in SW Iberia (Fig. 1a), developed in several segments of the Ossa-Morena Zone (OMZ), during the lower Palaeozoic (Variscan) opening of the Rheic Ocean (e.g., Nance et al. 2010; Ribeiro et al. 2007, 2010; Sánchez-García et al. 2003, 2010). An episode of carbonate sedimentation occurred in the north Gondwana margin during the Cambrian Series 2 (Gozalo et al. 2003; Liñán et al. 2004), well represented in the OMZ (Fig. 1b), intruded by igneous bodies during rift-related magmatic events that persisted until Lower Ordovician (e.g., Chichorro, et al. 2008; Dias da Silva et al. 2023; Díez Fernández et al. 2015; Sánchez-García et al. 2003, 2008, 2010, 2014), and by the Carboniferous syncollisional plutonism (e.g., Cambeses et al. 2019, 2021; Jesus et al. 2007; Lains Amaral et al. 2022; Pereira et al. 2017, 2022; Pin et al. 2008). The emplacement of such igneous bodies produced contact metamorphism during distinct Palaeozoic tectono-magmatic episodes and pose the question: What are the distinctive features and implications of this metamorphic overprint in the OMZ carbonate rocks? In addition, criteria to characterize the regionally metamorphosed marbles and the effect of late dolomitization is necessary to clearly separate the types of metamorphism (contact vs regional) and understand the extent of the role of accessory minerals in the development of calc-silicate minerals. This article presents a systematic study on the mineralogical and Sr-isotopic signature variations in carbonates from the central-northern region the OMZ during contact metamorphism resulting from Lower Palaeozoic rifting and Upper Palaeozoic synorogenic intrusions, as well as the late dolomitization processes.

Geological Setting

Carbonate rocks of the Ossa-Morena Zone

Carbonate sedimentation in the OMZ (Iberian Massif) manifested sparsely during four marine carbonate-production episodes from the Cambrian to the Devonian (Moreira et al. 2019), as well as in mixed siliciclastic-carbonate sedimentary basins during the Carboniferous (Armendáriz 2006; Cózar et al. 2006; González et al. 1990). The first episode of carbonate sedimentation took place during the Cambrian Series 2 (regional Ovetian-Marianian ages) related to rifting characterized by lithosphere thinning, synchronous with rift-related igneous events (Álvaro et al. 2014; Araújo et al. 2013; Gozalo et al. 2003; Liñán et al. 2004; Oliveira et al. 1991). Rifting in conjunction with the eustatic sea-level of the time generated a large carbonate platform environment, with microbial and archaeocyathan-microbial reef-like complexes (Álvaro et al. 2014; Gozalo et al. 2003; Liñán et al. 2004), which were responsible for producing the largest succession of carbonate rocks in the OMZ. This succession, known as the Detrital-Carbonate Group, is characterized by a sequence of calcite and dolomite limestones and marlstones interbedded with siliciclastic strata, metarhyolites and metabasalts (e.g., Sánchez-García et al. 2019).

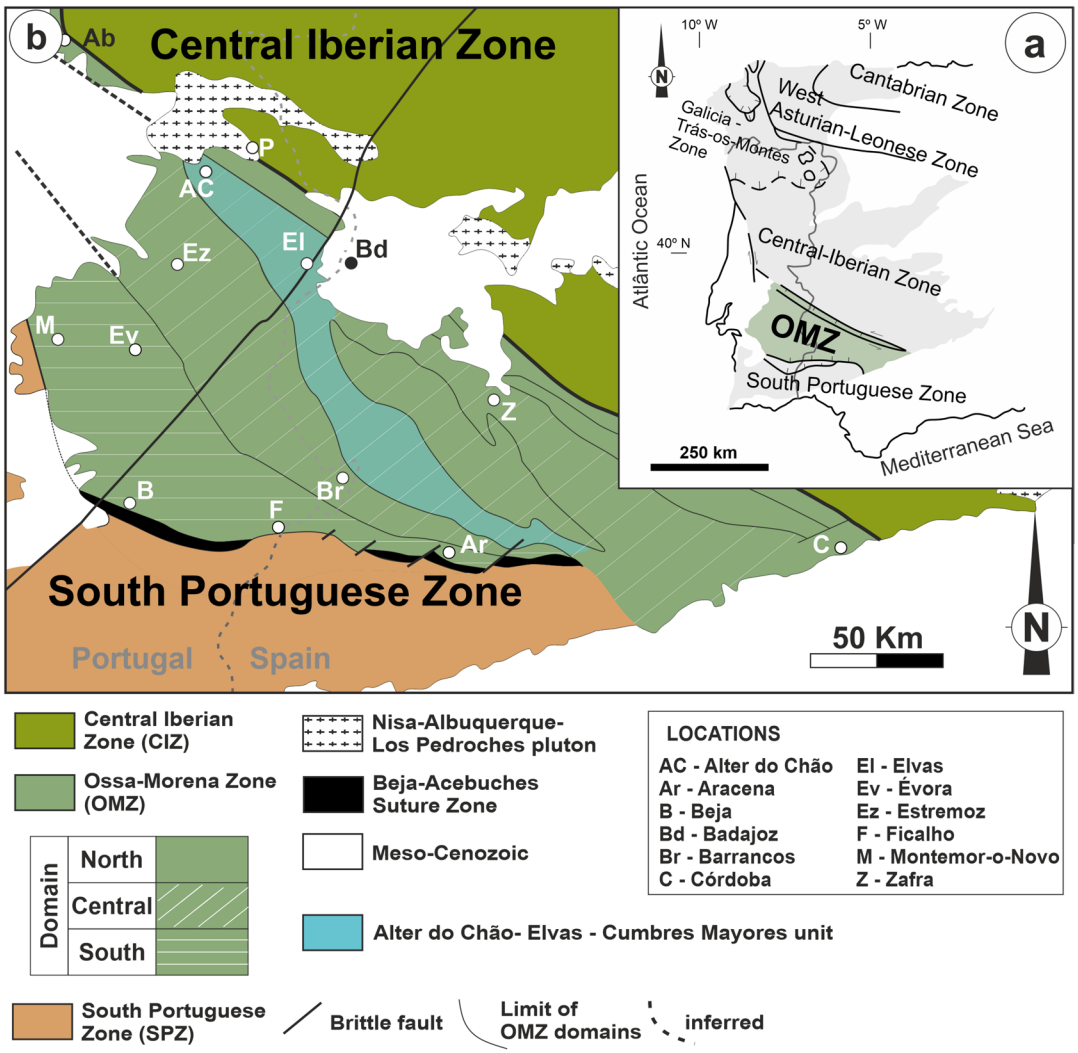

Fig. 1 **a** Tectonostratigraphic zonation of the Iberian Massif with the shaded area of Palaeozoic outcrops (adapted from Lotze 1945 and Julivert et al. 1974), highlighting the location of the Ossa-Morena Zone (OMZ). **b** Limits of the OMZ with the Central-Iberian Zone (in the northeast) and with the South Portuguese Zone (in the southwest), as well as its main domains (adapted from Robardet and Gutiérrez-Marco 2004), with emphasis on the studied Alter do Chão—Elvas—Cumbres Mayores unit in the central domain (Fig. 2). The northern OMZ domain corresponds to the Tomar-Badajoz-Córdoba Shear Zone and the Sierra Albarrana unit, the Central zone includes the Zafra-Córdoba-Alanís Unit, the Olivenza-Monesterio Antiform and the Montemor-Ficalho-Barrancos Hinolages unit, and the southern OMZ corresponds to the Beja-Aracena domain (Robardet and Gutiérrez-Marco 2004)

The second and third episodes of carbonate sedimentation have a much smaller expression and were formed contemporaneously with the drifting phase of the Variscan Cycle (Upper Ordovician and uppermost Silurian, respectively, e.g., Ribeiro et al. 2007). They are preserved in two synclines of the southern OMZ: the Valle and Cerrón del Hornillo synclines (Robardet and Gutiérrez-Marco 2004). In these synclines, a small Upper Ordovician carbonate unit, containing significant, often dolomitised and karstified bioclastic components, is exposed (late Katian stage, regional Kralodvorian). These limestones were generated during a warm climate event that preceded the global glaciation known as the Boda Event (e.g., Gutiérrez-Marco et al. 2019; Robardet and Gutiérrez-Marco 2004; Sarmiento et al. 2008, 2011). During the uppermost Silurian, a unit of black limestones interbedded with calcareous shales was deposited. This unit is representative of carbonate formation during anoxic/euxinic conditions from the Silurian Pridoli to the Lower Devonian Lochkovian (Gutiérrez-Marco et al. 2019; Robardet and Gutiérrez-Marco 2004). Other carbonate rocks attributed to the Silurian are also exposed in Portugal (Bencatel, Ferrarias, and Barrancos, among others; Moreira et al. 2019), though their ages are not well constrained (Moreira 2017; Piçarra and Le Meen 1994; Piçarra and Sarmiento 2006; Silvério et al. 2021). The last episode of carbonate sedimentation is a calciturbiditic reef system sequence

developed during the Devonian (Emsian to Givetian), which is mostly located in the southwestern domains of the OMZ (Machado et al. 2009, 2010, 2020; Oliveira et al. 2019), and in places associated with subduction-related basaltic rocks (Moreira et al. 2010; Silva et al. 2011). In some areas (i.e., Cabrela—Toca da Moura basins) these limestones are interpreted as olistoliths (Dias da Silva et al. 2024; Pereira et al. 2006), however this interpretation is not broadly recognized (Machado et al. 2020; Oliveira et al. 2019).

Most biostratigraphic records in the carbonate rocks from the four episodes have been partially obliterated by deformation and metamorphism, and their age constraints have only been attributed based on stratigraphic correlations (e.g., Araújo et al. 2013; Oliveira et al. 1991). This problem was addressed by Moreira et al. (2019) who applied strontium isotopic signatures to contextualize the marine carbonate events in time. They obtained $^{87}Sr/^{86}Sr$ ranges of 0.708299–0.708777 for Cambrian and 0.707680–0.707784 for Devonian limestones, congruent with worldwide seawater Sr isotopic record (e.g., Denison et al. 1997; Veizer et al. 1999). The $^{87}Sr/^{86}Sr$ ratios of the presumed Silurian limestones are inconclusive and partially overlap the Cambrian Series 2 (Ovetian–Marianian) signature (Moreira et al. 2019).

Tectono-magmatic and metamorphic events in the Ossa-Morena Zone

Two major superimposed periods of magmatic activity took place during the Variscan orogenic cycle, related to both the opening (rifting) of the Rheic Ocean (e.g., Sánchez-García et al. 2003, 2008, 2010, 2014) and later continental collision (e.g., Cambeses et al. 2019, 2021; Dias et al. 2002; Jesus et al. 2007, 2016; Pereira et al. 2022). Both rift-related and synorogenic magmatic stages are known to induce thermal metamorphism and consequently are responsible for the genesis of a set of contact calc-silicate rocks (s.l.) within the Series 2 Detrital-Carbonate Group throughout the OMZ (e.g., Carriedo et al. 2006; Chichorro 2006; Cruz 2013; Gonçalves 1971; Maia et al. 2022; Pereira 1999).

The rifting of northern Gondwana during the Cambro-Ordovician promoted the emplacement of numerous igneous suites throughout the Iberian Massif in three different phases: (i) an early event during the Terreneuvian (ca. 531–525 Ma; e.g., Chichorro, et al. 2008; Dias da Silva et al. 2023; Ochsner 1993; Pereira et al. 2011; Salman 2004; Sánchez-García et al. 2008, 2010, 2014) with the occurrence of calc-alkaline felsic to intermediate volcanic or volcanic-sedimentary rocks; (ii) a main bimodal event (Series 2 to Furongian, ca. 518–489 Ma, covering the first episode of carbonate production; e.g., Dias da Silva et al. 2023; Etxebarria et al. 2006; Ochsner 1993; Salman 2004; Sánchez-García et al. 2008, 2010; Sarrionandia et al. 2012), that comprises sets of sub-alkaline and alkaline mafic and felsic-intermediate volcanic and plutonic rocks, and iii) a later event that also includes bimodal igneous suites with alkaline and peralkaline volcanic rocks and plutons (Late Furongian to Floian, ca. 490–470 Ma; e.g., Ochsner 1993; Díez-Fernández et al. 2015; Sánchez-García et al. 2010).

Locally, syn-rift thermal metamorphism manifests as small aureoles around intrusions and migmatization in areas of extremely thinned crust, particularly in the central and northern regions of the OMZ, along the boundary with the Central-Iberian Zone, and in the Obejo-Valsequillo Domain. This is reflected by thermal domes associated with partial melting of Ediacaran metasedimentary rocks in the Valuengo, Monesterio and Lora del Rio metamorphic areas of the Olivenza-Monesterio Anticline (e.g., Expósito et al. 2003; Montero et al. 1999; Ordóñez-Casado 1998; Simancas et al. 2004), in the Mina Afurtunada region (Ordóñez-Casado 1998; Sánchez-García et al. 2008), in the Sierra Albarrana Domain (e.g., Solís-Alulima et al. 2020, 2023) and in the La Serena Massif (e.g., Moreno-Martín et al. 2023). The development of such thermal domes is concomitant with the emplacement of several rift-related magmatic rocks (Díez-Fernández et al. 2015; Sánchez-García et al. 2008; Simancas et al. 2004; Solís-Alulima et al. 2020).

Mafic volcanism associated with Devonian strata (Moreira et al. 2010; Ribeiro et al. 2010; Santos et al. 1990; Silva et al. 2011) and subsequent syncollisional (Tournasian-Visean) and post-collisional (Upper Pensilvanian-Cisuralian) intermediate-mafic and felsic intrusions (e.g., Cambeses et al. 2019, 2021; Dias et al. 2002; Jesus et al. 2007, 2016; Pereira et al. 2022) mark the convergent phase of the Variscan orogen. These intrusions are coeval with widespread progressive Barrovian metamorphism and were followed by Buchan metamorphism (e.g., Dias da Silva et al. 2018, 2023; Ribeiro et al. 2019, and references therein). Thermal domes were also developed syncollisionally, e.g., in the Évora and Aracena Massifs (Dias da Silva et al. 2018; Pereira et al. 2009) and in Ponte de Sor-Seda (Dias da Silva et al. 2023).

The Cambrian carbonate formation in Alter do Chão—Elvas—Cumbres Maiores unit of OMZ

Eustatic oscillations in the Cambrian during the opening of the Rheic Ocean had the utmost role in the development of the reef complexes that increased carbonate productivity, leading to the thick impure limestone sequences (e.g., Álvaro et al. 2014; Liñán et al. 2004; Oliveira et al. 1991). The Carbonate Formation (also referred to as Detrital-Carbonate Formation in Sánchez-García et al. 2019) outcrops in the Alter do Chão—Elvas—Cumbres Maiores unit of the OMZ (ACECMu; Robardet and Gutiérrez-Marco 2004) and is the largest exposed carbonate succession (variably metamorphosed) in the OMZ. It is composed of Cambrian

late Series 2 impure limestones, dolostones, marls, marbles, and calc-silicate rocks (s.l.), locally intruded by a variety of igneous bodies emplaced during the Cambro-Ordovician and Carboniferous (Fig. 2; Gonçalves 1971; Gonçalves and Assunção 1970; Gonçalves and Fernandes 1973; Gozalo et al. 2003; Liñán et al. 2004; Oliveira et al. 1991; Palacios et al. 2013). In the ACECMu, the bedding strikes from WNW-ESE to NNW-SSE, is moderately dipping to the NE and is often folded. To the southeast of the ACECMu, it follows the geometry of the Monesterio Antiform, dipping moderately to steeply to the NE in the northern flank and to SW in the southern flank. The metamorphic grade varies from anchizone to greenschist facies (chlorite zone) with an increasing metamorphic grade towards the NW (Gonçalves and Assunção 1970; Gonçalves and Fernandes 1973; Mata and Munhá 1990; Moreira et al. 2019). This is congruent with the recrystallization features and the presence of accessory minerals identified in marbles unrelated to the intrusions, namely muscovite, biotite, chlorite, and albite (Moreira et al. 2019). Marbles that underwent contact metamorphism described in the literature contain epidote, tremolite, diopside, vesuvianite, and garnet (Andrade 2022; Cruz 2013; Gonçalves and Fernandes 1973).

The Furongian-Lower Ordovician magmatic rocks that intruded the Carbonate Formation and promoted the occurrence of metamorphic calc-silicate assemblages include the Alter do Chão and Elvas gabbro-diorite suites, the Alter Pedroso, Vaiamonte, Outeirão, Pombal-Varche, Falcato, Alcamins (Fig. 2a; Carrilho Lopes 2020; Díez Fernández et al. 2015; Gonçalves 1971), Almendral, Barcarrota and Jerez de los Caballeros peralkaline granitoids and mafic dykes (Fig. 2b; Etxebarria et al. 2006; Palacios et al. 2013; Sarrionandia et al. 2012). These peralkaline bodies were emplaced during extreme crustal extension (e.g., Díez-Fernández et al. 2015), also responsible for the development of the Cambro-Ordovician thermal domes exposed elsewhere in the OMZ (e.g., Expósito et al. 2003; Simancas et al. 2004). The Carboniferous syn- to post-collisional igneous bodies that intruded the Carbonate Formation are 1) the Visean Brovales, Burguillos del Cerro, and Valencia del Ventoso plutonic complexes near Jerez de los Caballeros, in the core of the Monesterio Antiform (Fig. 2b; e.g., Cambeses et al. 2015, 2019, 2021; Dallmeyer et al. 1995); and 2) the large Santa Eulália Plutonic Complex (SEPC; Fig. 2a) from Upper Pensilvanian-Cisuralian (Cruz et al. 2022; Pereira et al. 2017) between Alter do Chão and Elvas. In this region, The mineral assemblages in carbonate rocks with no spatial relation to igneous bodies are assumed to only represent the effect of regional metamorphism and later weathering and dolomitization processes. Rocks located near the intrusions that have developed calc-silicate assemblages and recrystallization textures are assumed to have been affected by contact metamorphism.

Sampling and methods

Carbonate rocks affected by contact metamorphism and metasomatism surrounding the Alter do Chão gabbro (Fig. 3a), the alkaline-peralkaline rocks of Falcato (Fig. 3b), Almendral (Fig. 3c) and Vaiamonte (Fig. 4), and in the vicinity of the SEPC (Figs. 4b, 5) are exposed. Marbles, dolostones and calc-silicate rocks (s.l.) of the Carbonate Formation outcropping throughout the ACECMu were collected for petrographic, mineralogic and $^{87}Sr/^{86}Sr$ analyses to constrain primary and modification features (Table 1). The data were compared with previously studied low-grade calcite marbles interpreted as geochemically representative of unaltered rocks in the central-northern OMZ, as well as with rocks that were affected by secondary dolomitization (samples VB-2, VB-12, VB-18 and ALT-1 from Moreira et al. 2019).

Polished thin sections were produced according to standard techniques in the laboratories of the Department of Geosciences of the University of Évora. Samples with carbonate minerals were stained using alizarin red solution, imparting a reddish hue to calcite crystals while other carbonate components (e.g., dolomite) maintained the original color (Ayan 1965).

Sample powder (grain size <63 μm) were analyzed by XRD in the HERCULES Laboratory (University of Évora) using ruker D8 Discover diffractometer with DaVinci geometry and Lynxeye linear detector to determine mineral compositions. Diffractograms were collected with 2θ ranging 3°–75°, with incremental steps of 0.05° (1 s/step). Mineral identification and semi-quantification were facilitated using the software DIFFRAC.SUITE EVA from Bruker (using the ICDD PDF-2 database), applying the Reference Intensity Ratio method (RIR; Hubbard et al. 1976; Hubbard and Snyder 1988). The mineralogical data obtained by XRD are available in Supplementary Information 1 (S1).

Strontium isotopic compositions were determined for the carbonate samples in the Laboratory of Isotope Geology of the University of Aveiro. Samples underwent leaching with 1 M CH_3COOH for 2 h at room temperature to facilitate $^{87}Sr/^{86}Sr$ isotopic ratio determination from only the carbonate phases. Approximately 0.1–0.2 g of each sample was dissolved in 10 mL of 1N acetic acid in a closed Teflon cup (Savillex®) on a heating plate at 150 °C. The resulting suspension was transferred to a centrifuge tube to isolate the undissolved residue and the supernatant solution was recovered, dried, and dissolved in heated 6 M HCL solution and subsequently in 7 M HNO_3 for strontium extraction by ion chromatography. The segregated strontium residue was then deposited on a central Ta filament with 0.5N H_3PO_4. Isotopic ratios were measured on a VG

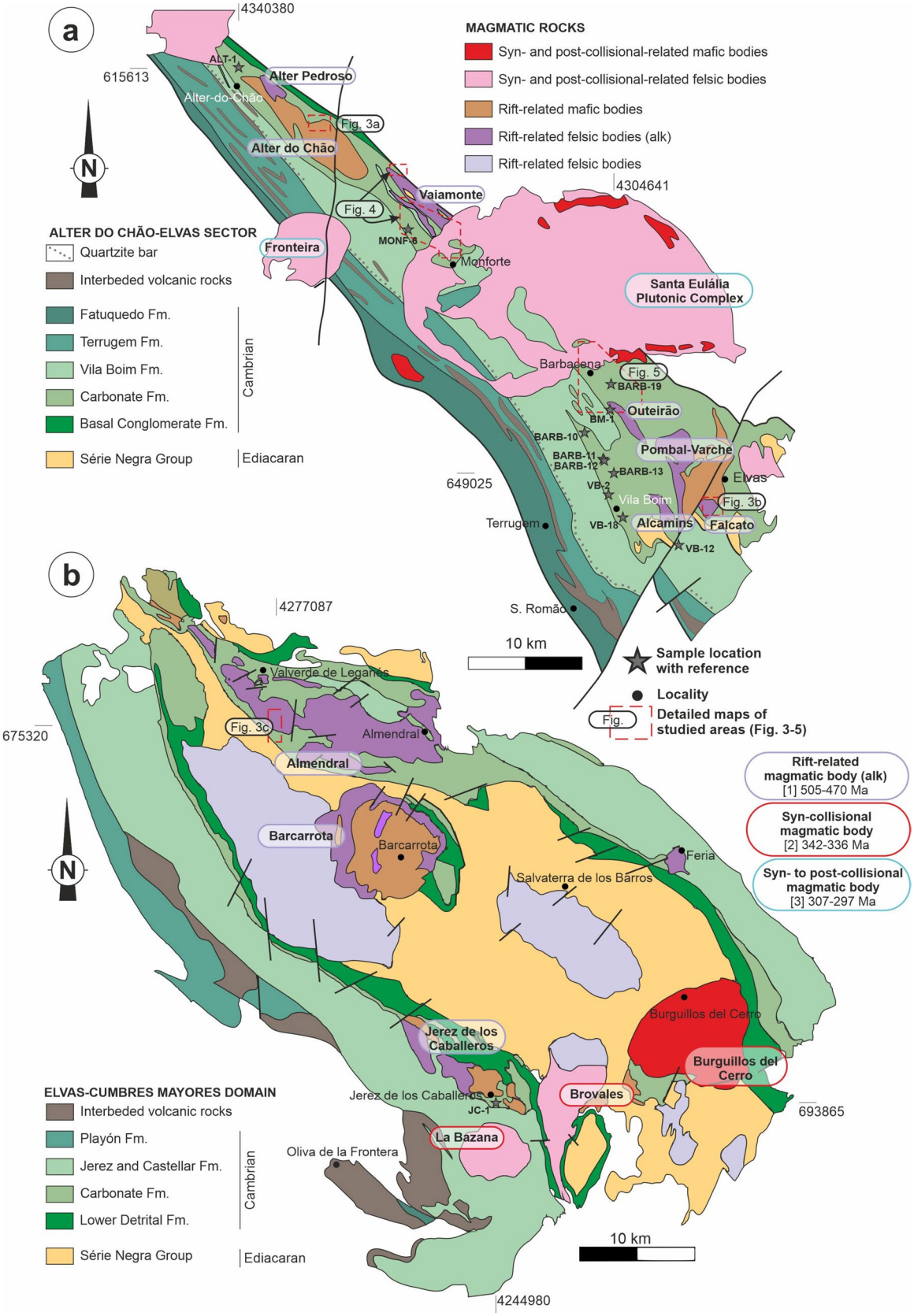
a
4340380
615613
4304641
649025
MAGMATIC ROCKS
Syn- and post-collisional-related mafic bodies
Syn- and post-collisional-related felsic bodies
Rift-related mafic bodies
Rift-related felsic bodies (alk)
Rift-related felsic bodies
ALTER DO CHÃO-ELVAS SECTOR
Quartzite bar
Interbeded volcanic rocks
Fatuquedo Fm.
Terrugem Fm.
Vila Boim Fm.
Carbonate Fm.
Basal Conglomerate Fm.
Série Negra Group
Cambrian
Ediacaran
ALT-1
Alter Pedroso
Alter-do-Chão
Fig. 3a
Alter do Chão
Vaiamonte
Fig. 4
MONF-8
Monforte
Fronteira
Santa Eulália Plutonic Complex
Barbadena
Fig. 5
BARB-19
Outeirão
BM-1
BARB-10
Pombal-Varche
BARB-11
BARB-12
BARB-13
VB-2
Elvas
Vila Boim
Fig. 3b
Terrugem
VB-18
Alcamins
Falcato
VB-12
S. Romão
10 km
Sample location with reference
Locality
Fig.
Detailed maps of studied areas (Fig. 3-5)
b
4277087
675320
693865
4244980
Valverde de Leganés
Fig. 3c
Almendral
Almendral
Barcarrota
Barcarrota
Feria
Salvaterra de los Barros
Rift-related magmatic body (alk) [1] 505-470 Ma
Syn-collisional magmatic body [2] 342-336 Ma
Syn- to post-collisional magmatic body [3] 307-297 Ma
Burguillos del Cerro
Jerez de los Caballeros
Burguillos del Cerro
Jerez de los Caballeros
JC-1
Brovales
La Bazana
Oliva de la Frontera
ELVAS-CUMBRES MAYORES DOMAIN
Interbeded volcanic rocks
Playón Fm.
Jerez and Castellar Fm.
Carbonate Fm.
Lower Detrital Fm.
Série Negra Group
Cambrian
Ediacaran
10 km

◂**Fig. 2** Geologic map of the Alter do Chão—Elvas—Cumbres Mayores unit of Ossa-Morena Zone (with sample locations and areas of detailed maps with contact metamorphism), showing **a** the Alter do Chão—Elvas Sector (Portugal) and **b** part of the Elvas—Cumbres Maiores Domain (Spain) with the Olivenza-Monesterio Anticline, Partially adapted from Gonçalves (1971) and Palacios et al. (2013). The "alk" rift-related felsic bodies are alkaline or peralkaline granitoid rocks, while other felsic bodies are calc-alkaline granites (peraluminous), mentioned in the text. Mafic rocks are gabbros and diorites. Ages from Díez Fernández et al. (2015) and Ochsner (1993) [1], Cambeses et al. (2019), Dallmeyer et al. (1995) and Errandonea-Martin et al. (2024) [2] and Cruz et al. (2022) and Pereira et al. (2017) [3]. Coordinate system: WGS84, UTM 29N

Sector 54 thermal ionization mass spectrometer (TIMS) in dynamic mode with beam intensities of 1–2 V for ^{88}Sr. The isotopic ratios were corrected according to the exponential fractionation law for the value $^{88}Sr/^{86}Sr = 0.1194$. The SRM-987 standard was analyzed along with the collected samples and the result provided a confidence interval of over 95%. All reagents used in the sample preparation were purified by double distillation. Ultra-pure water (18.2 MW cm) was obtained using a Milli-Q Element system (Millipore). This procedure follows that of Moreira et al. (2019) who also conducted carbonate rock analysis for the OMZ.

Mineralogical and petrographic features of the ACECMu

Rocks that underwent regional metamorphism

The carbonate rocks located far from the intrusions are assumed to represent the effects of regional metamorphism (samples BM-1, MONF-6, BARB-13, BARB-19) and commonly preserve bedding features. However, in thin section they appear massive, with no visible internal primary structures. Petrographically, these marbles show very fine to medium grain size in a granoblastic polygonal texture and do not have calc-silicate phases in their composition (Figs. 6a–b and 8). Calcite is the dominant phase (>50% in the mineral assemblage), preserved as subhedral-anhedral crystals with evidence of bulging and ductile recrystallization of calcite (e.g., Fig. 6a–d). The modal abundance of accessory silicate mineral assemblage and mode varies (Fig. 8), and consists mainly of quartz, feldspars (plagioclase and minor K-feldspar) and muscovite with minor chlorite, clays, and opaque minerals. Sample BM-1 exhibits twinned calcite and rare twinned dolomite crystals (Fig. 6c), and rare late dolomite rhombs (Fig. 6d). Calcite twins appear only in coarse grain samples and vary between type I and type II, with crystals showing narrow and wider twin thickness randomly through the rock (Fig. 6a–b).

Rocks that underwent late dolomitization

Dolomite-rich rocks (JC-1, BARB-10, BARB-11 and BARB-12) preserve fine-grained cloudy late dolomite, occasionally displaying subhedral to euhedral rhomb contours growing over the primary carbonate and accessory minerals (Fig. 6d–f). Dissolution patches may be associated with euhedral-subhedral crystals (Fig. 6e–f). The dolomite totally or partly obliterates the original textures, indicating secondary growth. The occurrence of secondary dolomite, in carbonate rocks not affected by contact metamorphism, was reported by Moreira et al. (2018, 2019).

Contact metamorphism associated with rift-related gabbros

Samples BAT-1 and BAT-2 were collected near the Alter do Chão gabbroic massif (Fig. 3a). The rocks are composed of K-feldspar (25.3–39.7%), diopside (12.2–18.7%), scapolite (4.2–23.3%) and calcite (10.4–13.2%). Scapolite crystals occur as large irregular porphyroblasts in a groundmass of diopside, quartz, feldspar, and calcite.

Contact metamorphism associated with rift-related alkaline-peralkaline granitoids

Samples FALC-3A and FALC-F3 were collected from two different locations in the Falcato peralkaline massif (Fig. 3b). In the northern enclave (FALC-3A), rocks adjacent to the intrusion are substantially composed of silicates, namely garnet (38.4%), plagioclase (24.1%), quartz (17.7%), and diopside (17%), with minor calcite (2.9%, with patchy type IV twin; Fig. 7e–f). Garnet occurs as blasts surrounding carbonates, while epidote, calcite and quartz appear within garnet cores, filling dissolution holes and cracks (Fig. 7e). On the eastern contact, sample FALC-F3 contains dominant calcite (70.4%) forming irregular-shaped crystals in a mosaic texture frequently with tenuous type II twins, and subordinate amounts of pargasite (19.4%) and feldspars (plagioclase = 3.5%; K-feldspar = 6.7%) (Fig. 7g).

Samples related to the Almendral body were collected from a roof pendant (Fig. 3c). In the inner part of the roof pendant, sample VLA-1 show higher carbonate mineral abundance (calcite = 76.6%, with type I and type II twins) and low percentage of calc-silicate phases (tremolite = 5%), while sample VLA-3, collected closer to the intrusion, contains a smaller proportion of calcite (55.3%, with irregular untwinned crystals) and greater amount of calc-silicate minerals (diopside = 13.9%, scapolite = 9.8%). In the intermediate area, sample VLA-2 only contains diopside (12.3%) and garnet (18.7%) within a very retrogressed epidote-rich matrix. The garnet, anisotropic under polarized light (also described in unusual cases,

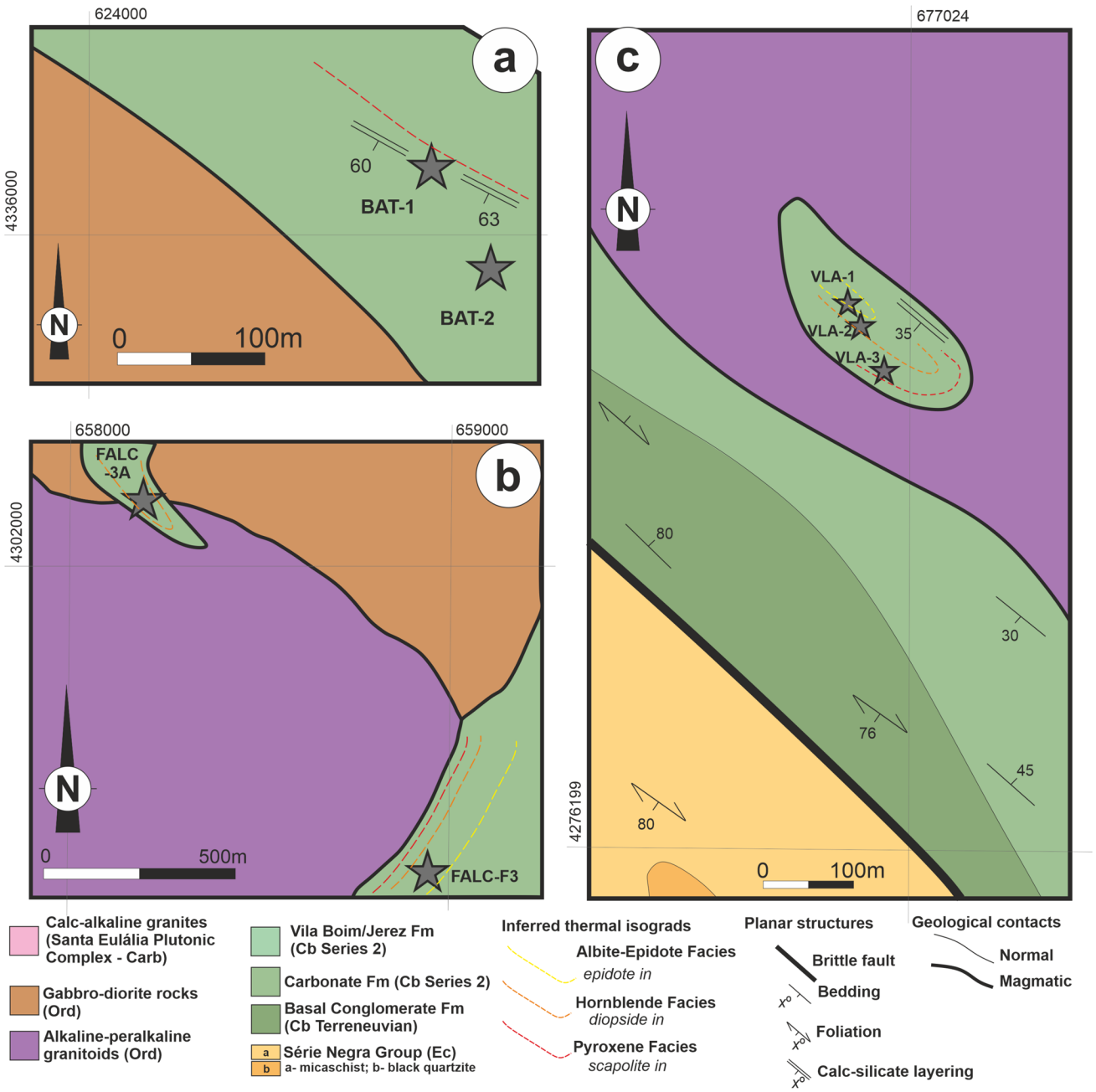

Fig. 3 Detailed geologicl maps with location of the studied samples associated with igneous intrusions from ACES and ECMD, including structural features. **a** Samples collected near the Alter do Chão gabbro. **b** Samples associated with the Falcato peralkaline massif, in the northern enclave and in the eastern contact. **c** Samples from the roof pendant from the Almendral body. Maps partially adapted from Gonçalves and Assunção (1970), Gonçalves and Fernandes (1973) and Muelas Peña et al. (1976)

e.g., Rossman and Aines 1991), occurs as aggregates or very fractured in a calcite-epidote retrogression matrix (Fig. 7h) or as atolls around calcite and epidote crystals. Rare fluorite occurs as an accessory in an epidote-calcite vein. Samples VLA-3A and VLA-3B, collected near the intrusion are mostly composed of carbonate minerals with few calc-silicate phases (carbonate fraction >90% and calc-silicates <3.5%).

The silicates consist of accessory chlorite, K-feldspar, tremolite, dolomite, mica (muscovite) and epidote and, in these two samples, calcite often shows intersecting type I and type II twins, sometimes curved (type III).

Samples VCS-1, VCS-3, VCS-4 (northern limit, Fig. 4a) and MONF-7, MONF-8, MONF-9 (southern limit; Fig. 4b) were collected from the vicinity of the Vaiamonte peralkaline body, are characterized by various assemblages, often

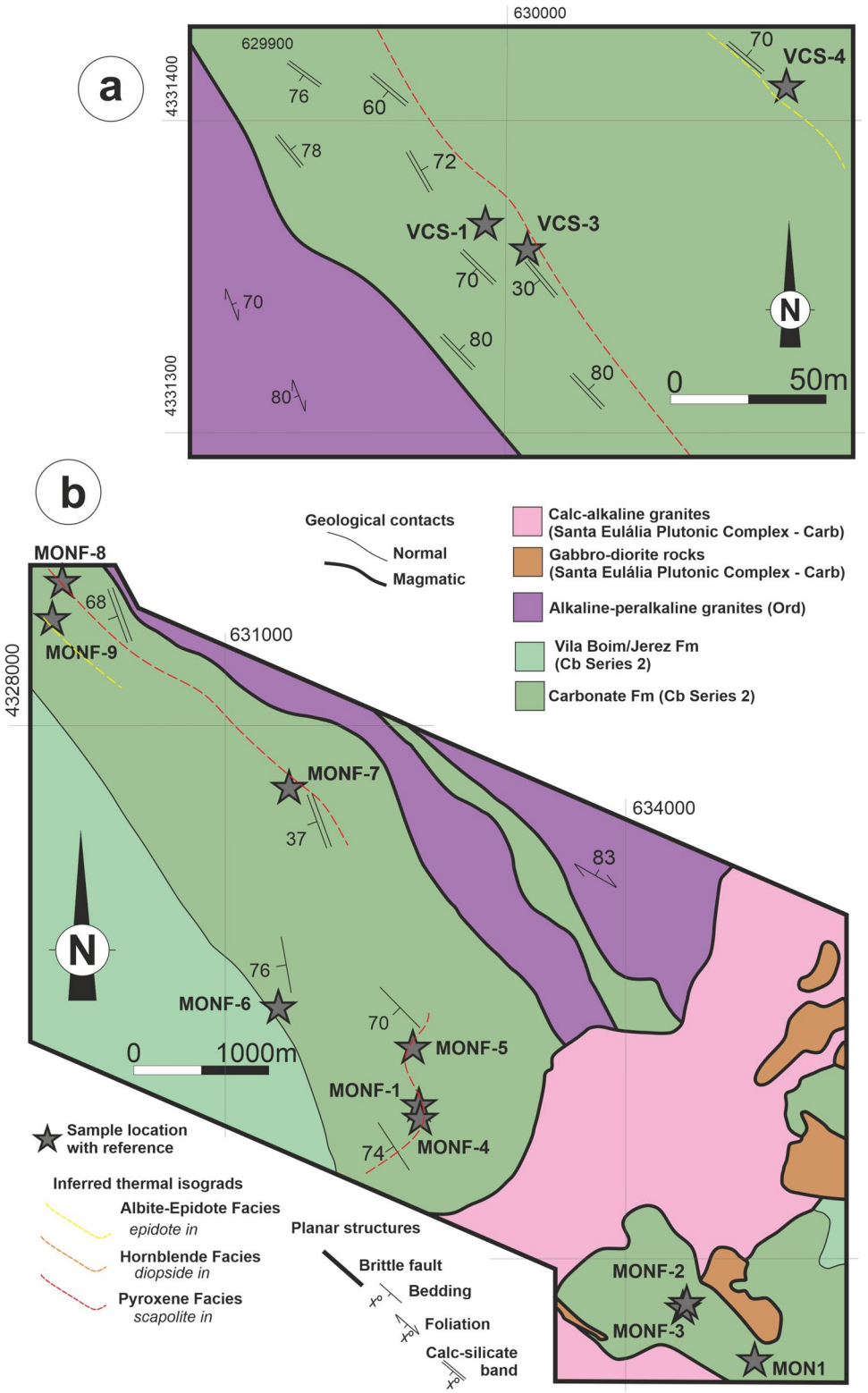

Fig. 4 Detailed geologic maps with the location of the studied samples related to igneous intrusions associated with the Vaiamonte body and the SEPC, including structural features **a** Sample localities near the northern border of the Vaiamonte igneous rocks. **b** Map of the Monforte area, with sample localities close to the southern border of the Vaiamonte body, and samples associated with the SEPC located on the country rocks and in the roof pendant. Partially adapted from Gonçalves and Fernandes (1973)

developing a calc-silicate layering (Fig. 7a–b). The samples from the northern limit display a decrease of the carbonate fraction with an increment of the calc-silicate phases (scapolite and tremolite) from the outer zone (VCS-4, calcite + dolomite = 82.2%; tremolite = 6.1%) to the proximity of the intrusion (VCS-3, carbonates = 12.3%; scapolite + tremolite = 46.6%; VCS-1, carbonates = 2.4%, scapolite + tremolite = 74.7%). The southern border also shows a

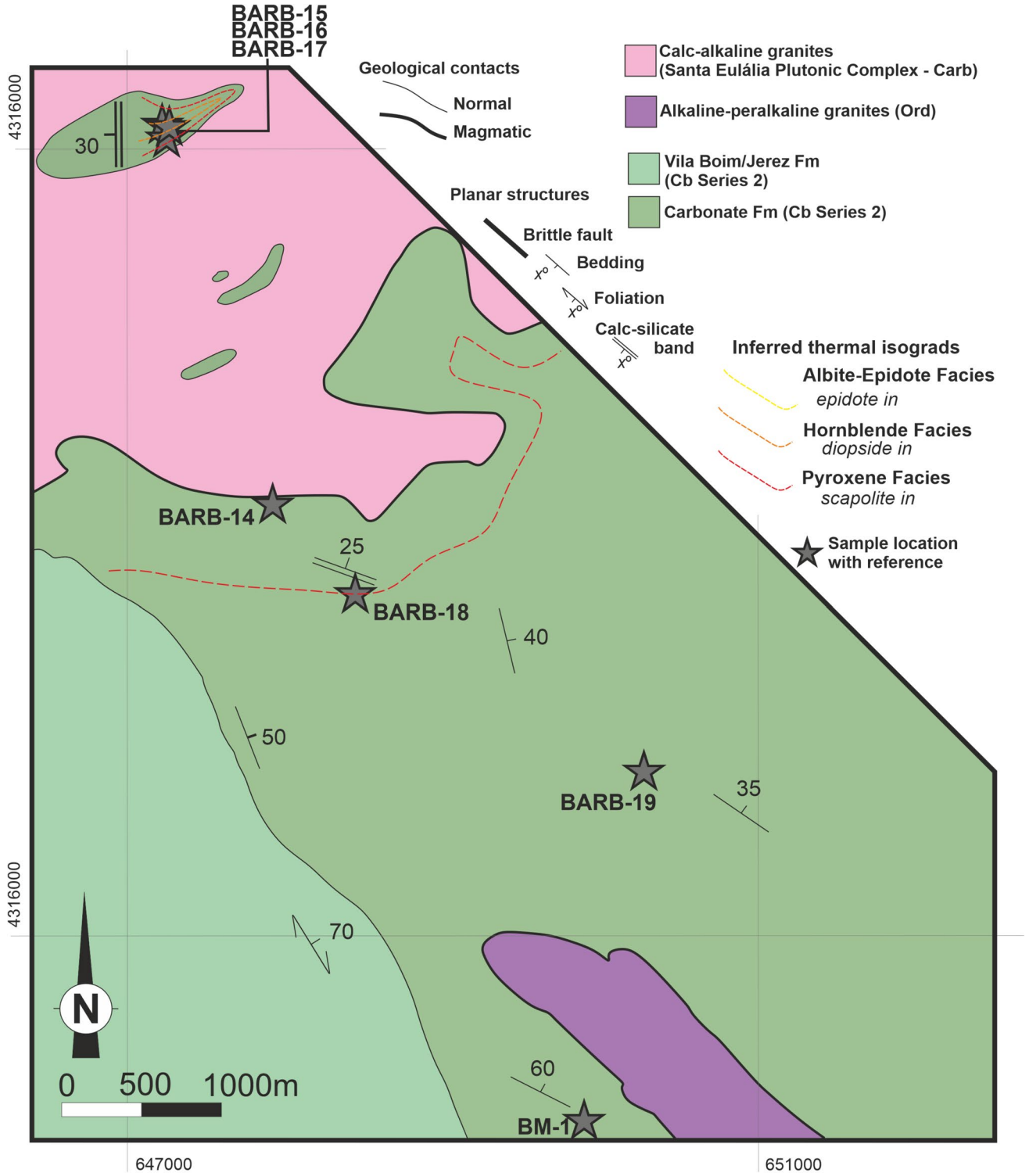

Fig. 5 Map of the rocks collected in the southeastern limit of the SEPC, with samples from intrusion-unrelated marbles, and rocks associated with the Santa Eulália Plutonic Complex. Adapted from Gonçalves and Assunção (1970)

similar pattern, with a decrease in the carbonate abundance towards the intrusion, compensated by the growth of calc-silicate phases. The main difference between these segments lies in the nature and abundance of calc-silicate minerals: abundant tremolite (northern limit), and talc, chlorite, and albite (southern limit) (Fig. 8). Epidote and plagioclase are

Table 1 Location and field classification of studied rocks

	Ref:	Latitude	Longitude	Field classification
Not related to intrusions				
Calcite low-grade marbles				
Outeirão	BM-1	38.922890	−7.269210	Calcite–dolomite low-grade marble
Vila Boim	VB-2*	38.861410	−7.282240	Calcite low-grade marble
Vila Boim	VB-18*	38.836930	−7.261980	Calcite low-grade marble
Monforte	MONF-6	39.071940	−7.481600	Calcite low-grade marble
Barbacena	BARB-13	38.877660	−7.281560	Calcite low-grade marble
Barbacena	BARB-19	38.944410	−7.266050	Calcite low-grade marble
Late dolomitized marbles				
Alter do Chão	ALT-1*	39.204930	−7.660690	Dolostone
Vila Boim	VB-12*	38.826580	−7.215970	Dolostone
Jerez de los Caballeros	JC-1	38.332190	−6.782980	Dolostone
Barbacena	BARB-10	38.911930	−7.304480	Dolostone
	BARB-11	38.890630	−7.292070	Dolostone
	BARB-12	38.890630	−7.292070	Dolostone
Related with intrusions				
Related to alkaline felsic rocks				
Falcato	FALC-3A	38.854230	−7.178380	Garnet-rich calc-silicate rock
	FALC-F3	38.843860	−7.167630	Calcite marble
Vaiamonte (NW)	VCS-1	39.121780	−7.496360	Banded calc-silicate rock
	VCS-3	39.121240	−7.496090	Epidote-rich calc-silicate rock
	VCS-4	39.122160	−7.495240	Calcite–dolomite marble
Vaiamonte (SE)	MONF-7	39.087020	−7.479920	Calcite–dolomite marble
	MONF-8	39.101190	−7.500840	Calcite–dolomite marble
	MONF-9	39.099200	−7.500240	Calcite marble
Almendral	VLA-1	38.625840	−6.985720	Calcite–epidote marble
	VLA-2	38.625400	−6.985560	Epidote-fluorite calc-silicate rock
	VLA-3	38.624660	−6.985340	Calcite–epidote marble
	VLA-3A	38.624660	−6.985340	Calcite marble
	VLA-3B	38.624660	−6.985340	Calcite marble
Related to gabbroic rocks				
Alter do Chão	BAT-1	39.164780	−7.562210	Calc-silicate rock
	BAT-2	39.164150	−7.561580	Banded calc-silicate rock
Related to post-collisional granitoids				
Santa Eulália Plutonic Complex	MONF-1	39.064790	−7.469180	Calcite marble
	MONF-4	39.064570	−7.469150	Calcite marble
	MONF-5	39.069320	−7.469530	Calcite marble
	BARB-14	38.960830	−7.293180	Calcite marble
	BARB-18	38.954870	−7.286850	Calc-silicate rock
	MON-1	39.047540	−7.440530	Calcite marble
	MONF-2	39.051320	−7.446560	Calcite marble
	MONF-3	39.051320	−7.446560	Calcite-Vesuvianite marble
	BARB-15	38.981750	−7.301340	Banded calc-silicate rock
	BARB-16	38.981750	−7.301340	Banded calc-silicate rock
	BARB-17	38.981750	−7.301340	Calcite marble

*Samples from Moreira et al. (2019). Coordinate system: WGS84, UTM 29N

common phases but are not always detected by XRD. Scapolite often occurs as irregular porphyroblasts with low relief, associated with plagioclase with epidote inclusions (Fig. 7c) or as large blasts growing over the fine epidote matrix (Fig. 7d). The geometry of calcite twinning is dominated by type I and II twins, more often observed in coarse-grained

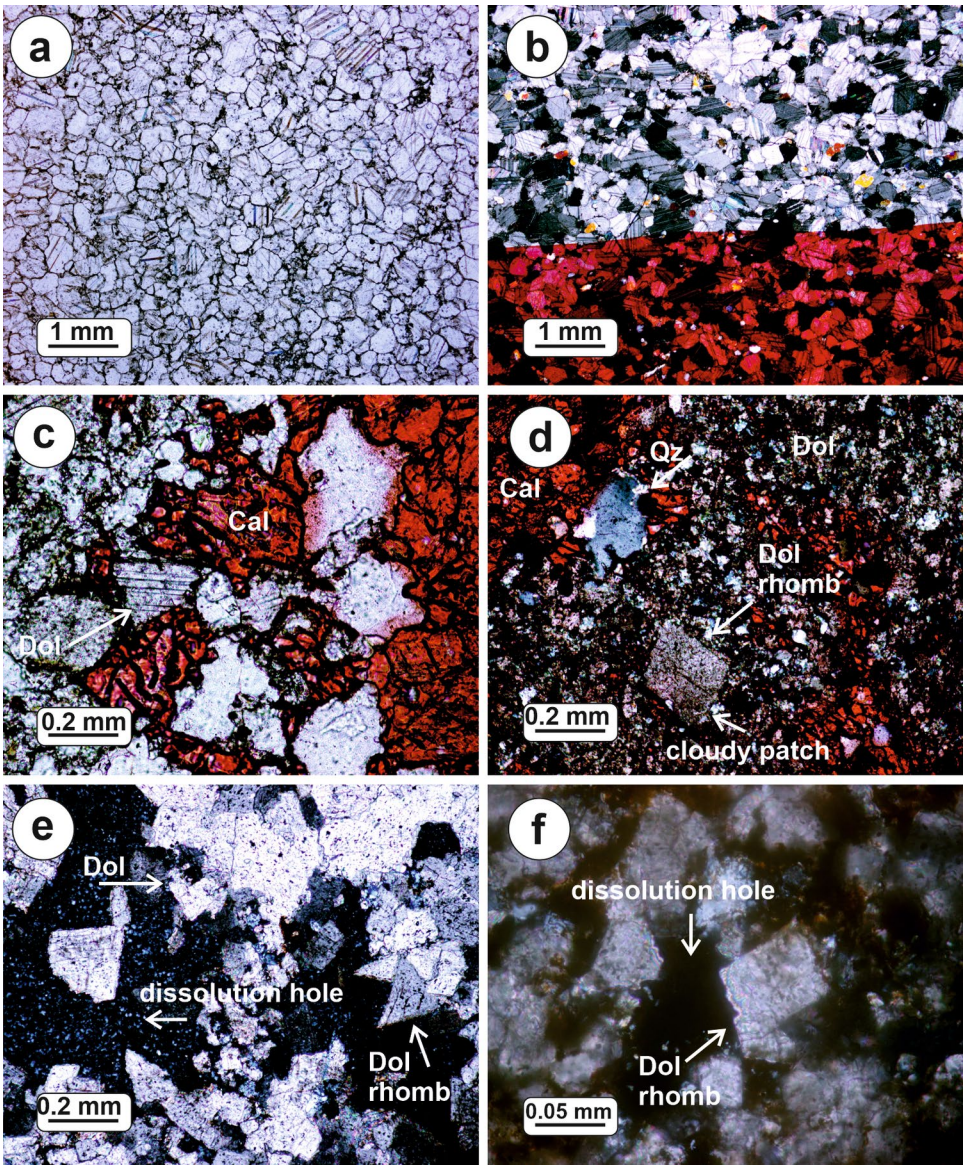

Fig. 6 Photomicrographs of petrographic aspects of the samples assumed unaffected by the intrusin. **a** Generic aspects of pure calcite marble (regionally metamorphosed), displaying the inequigranular granoblastic polygonal texture and type I and II calcite twins (sample MONF-19). **b** Confirmation of the calcite fraction with the Alizarin Red solution in sample MONF-6. **c** Subhedral calcite and dolomite crystals in polygonal fabric, in which dolomite presents twinning (sample BM-1). **d** Coeval calcite and dolomite crystals in medium-fine mass, with growth of a dolomite rhomb with a cloudy appearance in sample BM-1. **e** Rhomb and anhedral dolomite crystals next to large dissolution holes from JC-1. **f** Euhedral dolomite rhomb next to dissolution hole in sample BARB-11

samples. In both areas, samples with an assemblage typical of albite–epidote facies (VCS-4 and MONF-9) show a larger percentage of dolomite (10.7 and 25.5%), while samples with scapolite contain no dolomite.

Contact metamorphism related to the Santa Eulália Plutonic Complex

The samples related to the Santa Eulália Plutonic Complex were collected from the northwestern (MONF-1, MONF-4 and MONF-5; Fig. 4b) and southeastern (BARB-14 and BARB-18; Fig. 5) part of the metamorphic aureole, as well as from the roof pendants (MON-1, MONF-2, MONF-3, BARB-15, BARB-16 and BARB-17; Figs. 4b and 5). Samples MONF-1, MONF-4 and MONF-5 have dominant silicate mineral composition, constituted by mica (46.3–58.6%), with subordinate amounts of calc-silicate minerals (scapolite >3.7%, and epidote >0.9%); the carbonate fraction varies between 20.1–38.3%. In the southeastern part, sample BARB-14 is composed mostly of dolomite (85.8%, out of 99.6% carbonate fraction) and remnant chlorite (0.2%) and plagioclase (0.3%), while BARB-18 is a calc-silicate rock, containing a predominance of the calc-silicate minerals diopside (26.6%), scapolite (24.1%) and vesuvianite (3.6%), with less calcite (20%). The samples collected from the roof pendants show substantial mineralogical variability, from carbonate rocks (MON-1, MONF-2, MONF-3 and BARB-17) formed mostly by calcite (65.8–81.8%), to rocks almost solely consisting of calc-silicate phases and feldspars (BARB-15 and BARB-16; Fig. 7i). Calc-silicate mineral assemblage on roof-pendant samples contain common diopside (2.1–25.5%, in all samples), scapolite

(2.1–45.9%, MON-1, BARB-15 and BARB-16) and vesuvianite (3.6–16.7%, on MONF-2 and MONF-3), as well as rare wollastonite (10.1%, on BARB-15, though not identified petrographically) (Fig. 7j). Veinlets with coarse-grained carbonate and diopside crystals usually cut the altered marbles (Fig. 7k).

Carbonate and calc-silicate nomenclature for the carbonate formation rocks

The analyzed mineralogical composition of the Carbonate Fm is presented in Fig. 6, which shows significant heterogeneity in the carbonate fraction (Fig. 8a), calc-silicate assemblages and other non-carbonate minerals (Fig. 8b). The samples are grouped according to their mineralogical features in typical OMZ regionally metamorphosed marbles, marbles with late dolomite and rocks with calc-silicate mineralogy. Some Ca-poor silicate phases, namely quartz, mica (muscovite or biotite), albite and K-feldspar are common in all types of samples, while calc-silicates only appear in samples spatial associated with intrusions. The ternary classification plots show that rocks distant from igneous bodies with calcite dominant over dolomite and silicate fraction composed only of quartz, mica and feldspars correspond to rocks derived from impure limestones, while the rocks with dominant cloudy dolomite plot in the varying fields of impure and pure dolostones (Fig. 9a). Overall, the samples with no calc-silicate minerals consist of impure marbles with variable mineralogy (Fig. 9b). Samples associated with the intrusions have a wide range of composition, varying from high-carbonate fractions (derived from calcitic dolostone or dolomitic limestone, Fig. 9a), to rocks mostly embodied by silicate minerals (from calc-silicate-bearing impure marbles to calc-silicate *s.s.* rocks, Fig. 9b). Most of these samples fall within the 'carbonate–silicate rock' field, with modal silicate fraction between 50–95%, and only three samples (VCS-1, BARB-15, and FALC-3) are classified as calc-silicate rocks s.s., with <5% carbonates and >50% calc-silicates over the common mineralogy (Fig. 9b).

Sr-isotope values of carbonates from the ACECMu

The $^{87}Sr/^{86}Sr$ analyses for the carbonate samples are presented in Table 2, and plotted according to mineralogical abundance and nearby intrusion in Fig. 8. Samples with very low-carbonate fraction (FALC-3A, VCS-1, BARB-15; carbonate minerals <5%) were not analyzed.

Intrusion-unrelated calcite marbles show a low $^{87}Sr/^{86}Sr$ ratio (0.70832–0.70877), while dolostones show higher values (0.70887–0.70955). The samples collected near the intrusions yielded more variable results:

- The two low-carbonate samples collected near the Alter do Chão gabbro (BAT-1 and BAT-2), yield high $^{87}Sr/^{86}Sr$ values (0.70906–0.70939).
- The carbonate sample next to the Falcato massif (FALC-F3) yielded $^{87}Sr/^{86}Sr = 0.70876$.
- The rocks collected from the roof pendant of the Almendral massif yielded $^{87}Sr/^{86}Sr$ values that appear unrelated to the sample location: $^{87}Sr/^{86}Sr = 0.70876$ in the centre (VLA-1), $^{87}Sr/^{86}Sr = 0.70953$ in the intermediate zone (VLA-2), and $^{87}Sr/^{86}Sr = 0.70869$ near the contact (VLA-3). Rocks near the contact composed of dominant calcite (VLA-3A) or coeval calcite–dolomite (VLA-3B) with very little calc-silicate phases yield consistently lower ratios of 0.70838 and 0.70841, respectively.
- In the northern limit with the Vaiamonte intrusive, $^{87}Sr/^{86}Sr$ vary from 0.70815 (VCS-1) to 0.70911 (VCS-3), while in the southern border the ratios are slightly higher, ranging from 0.70854 (MONF-9) to 0.70959 (MONF-8).
- In the low-carbonate samples (<50% carbonates) collected from the NW contact of the SEPC granite, $^{87}Sr/^{86}Sr$ range from 0.70853 (MONF-4) to 0.70869 (MONF-1) and 0.70876 (MONF-5). On the SE border, samples yielded more variable $^{87}Sr/^{86}Sr$ results, which vary from 0.70836 (BARB-14, lowest value of the group) to 0.70943 (BARB-18, with the highest value). A somewhat coherent span of values was determined in samples from the roof pendants, ranging 0.70850 (MON-1), 0.70852 (MONF-2) and 0.70857 (MONF-3) in the western roof pendant, and a broader range of 0.70846–0.70878 (BARB-16) in the eastern roof pendant.

Discussion

Regional metamorphism and late dolomitization overprint

The Cambrian impure marbles commonly contain dominant calcite or coexisting calcite–dolomite with accessory quartz, feldspar and mica and no trace of calc-silicate minerals. The recrystallization of the calcite during regional metamorphism is assumed to have obliterated most of the primary or sedimentary structures. In some samples, the strong secondary dolomitization of the rocks from the Carbonate Formation is interpreted to have taken place after burial, i.e., after diagenesis and the regional Variscan metamorphic stage, by the action of meteoric or high salinity waters (e.g., Moreira et al. 2019). The dolomite rhomb that has grown over a dolomite-rich marble (sample BM-1; Fig. 6d), suggests that the dolomitizing event occurred after regional metamorphism. The significative amounts of quartz and mica in both the calcite-rich and dolomitized marbles confirm that

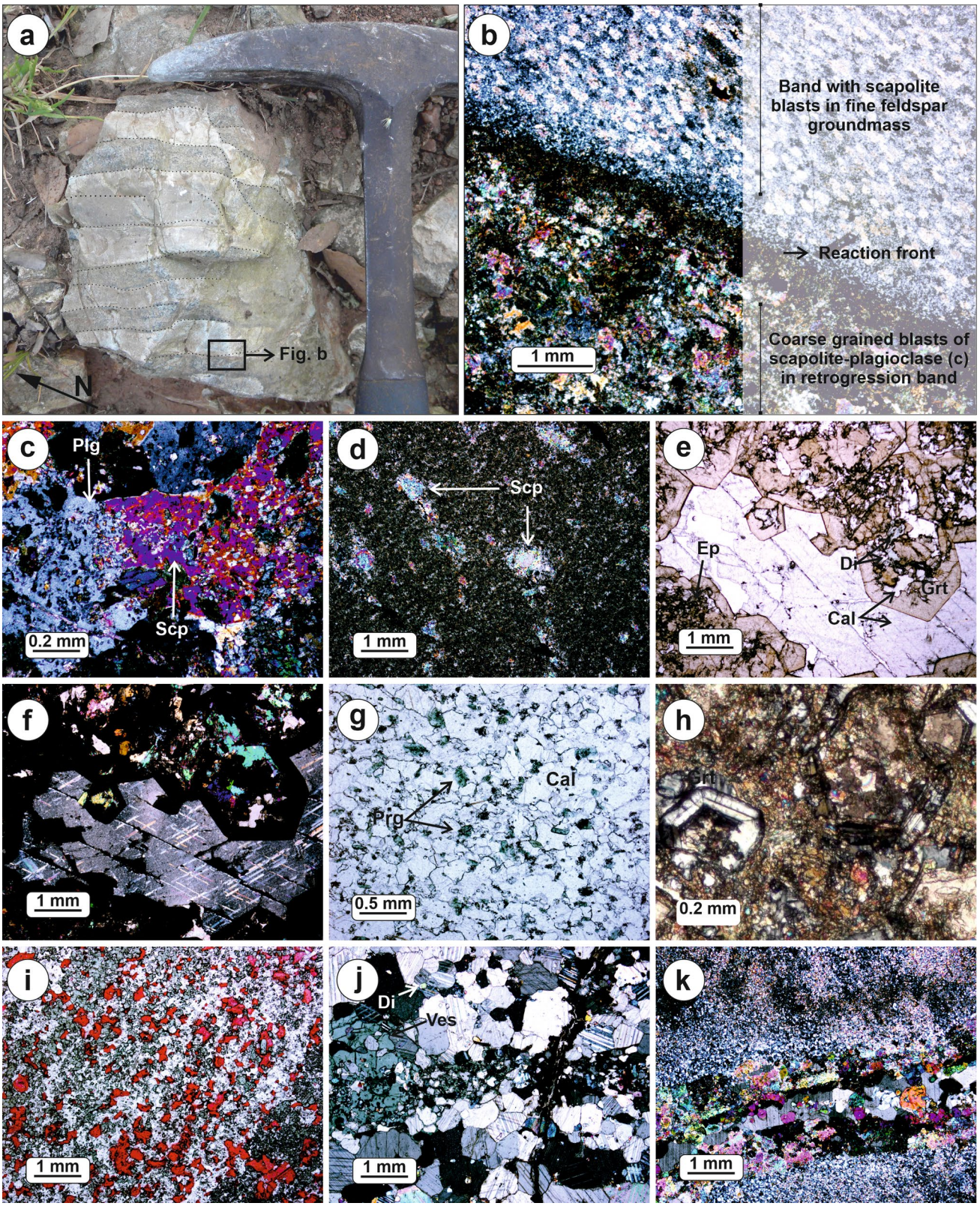
a
Fig. b
N
b
1 mm
Band with scapolite blasts in fine feldspar groundmass
Reaction front
Coarse grained blasts of scapolite-plagioclase (c) in retrogression band
c
Plg
Scp
0.2 mm
d
Scp
1 mm
e
Ep
Di
Grt
Cal
1 mm
f
1 mm
g
Cal
Prg
0.5 mm
h
Grt
0.2 mm
i
1 mm
j
Di
Ves
1 mm
k
1 mm

◂**Fig. 7** Distinct textural and mineralogical aspects of rocks bearing calc-silicate minerals. **a** Outcrop of rock with calc-silicate bands in Vaiamonte body (VCS-1). **b** Photomicrograph of contact between calc-silicate layers, showing scapolite + feldspar + quartz rich band and scapolite + plagioclase + epidote retrogressed band. **c** Photomicrograph of an example of the scapolite and plagioclase relationship, both with epidote inclusions (VCS-3). **d** Photomicrograph of scapolite porphyroblast in a sample from the S limit of Vaiamonte body (MONF-8). **e** Photomicrograph showing euhedral garnet around calcite. Garnets are very fractured and contain epidote, diopside, calcite and quartz growing from dissolution zones and cracks in the core (FALC-3A). **f** Crossed-polar image of the same sample (FALC-3A), emphasizing the calcite thick type-IV twins, patchy or interrupted. **g** Photomicrograph showing polygonal calcite grains with irregular shapes and low-relief pargasite near calcite boundaries (Falc-F3). **h** Crossed-polar photomicrograph of anisotropic garnet fragment and atoll filled with groundmass minerals (calcite and epidote) (VLA-2). **i** Calcite dispersion highlighted by the Alizarin Red solution on the calc-silicate arrangement (BARB-16). **j** Photomicrograph of vesuvianite marble sample from the SEPC, showing inequigranular mosaic of irregular calcite (with type I and II twins) and vesuvianite aggregates (MONF-3). **k** Calcite-diopside vein on fine-grained calc-silicate (BARB-16)

the regional metamorphism in this sector did not exceed the chlorite zone/lower greenschist facies (as described by Moreira et al. 2019). Additionally, the dominant calcite type I and II twins (Fig. 6a–b) and rarer unaltered dolomite twin (sample BM-1; Fig. 6c) suggest maximum temperatures of around 300 °C (e.g., Passchier and Trouw 2005).

The near total replacement of primary calcite by dolomite (often rhombohedral and with rare cloudy patches; Fig. 6d–f) appears to have occurred while quartz, muscovite and to a lesser extent chlorite and feldspars were preserved (see also Moreira et al. 2019). Typical regionally metamorphosed marbles with no evidence of dolomitization yield carbonate fraction $^{87}Sr/^{86}Sr$ similar to those expected from the $^{87}Sr/^{86}Sr$ isotopic curve of Cambrian Series 2 seawater. In contrast, when secondary dolomite is the dominant phase, the $^{87}Sr/^{86}Sr$ are noticeably higher, with an apparent boundary at around $^{87}Sr/^{86}Sr = 0.7088$ (Figs. 10, 11b). Dolomitization is interpreted to be the result of the post-metamorphic interaction with meteoric, saline or other shallow fluids, and the $^{87}Sr/^{86}Sr$ ratio is dependent on the composition of the surrounding rocks that compose the drainage basin, the climatic conditions, and the evaporation rates. The significant increase of the $^{87}Sr/^{86}Sr$ ratio coud also have been caused if the dolomitizing fluids resulted from the mixing of waters derived from high $^{87}Sr/^{86}Sr$ sources like upper crustal rocks and pelagic sediments, and/or achieved higher values by evaporative concentration (e.g., Faure and Mensing 2005; Moreira et al. 2018, 2019; Rollinson and Pease 2021). Therefore, $^{87}Sr/^{86}Sr$ values between 0.7083 and 0.7088 may represent the primary/diagenetic signature for Cambrian limestones of the Carbonate Formation (Fig. 10), while the higher values are likely explained by secondary late dolomitization.

The calcite marbles throughout the region have no proximity to igneous bodies, and therefore the mineralogical and isotopic results are interpreted as representative of the composition of the protolith. However, as the dolomitization appears to have been "late", occurring after diagenesis and metamorphism, rocks exhibiting late dolomitization will not be considered further here.

Effects of contact metamorphism on the protolith

Mineralogical changes

The textural and mineralogical transformation of the Carbonate Formation during contact metamorphism from the two different tectono-magmatic events during the Variscan Cycle are noteworthy from outcrop to microscopic scale. The overprint of calc-silicate minerals is expressed in the external contact aureoles of igneous bodies and enclaves/roof pendants, with notable growth of assemblages as fracture-filling veins, texture overgrowth, and replacement of previous fabrics. The metamorphic effects related to the time-separated Cambro-Ordovician and Carboniferous intrusions may have developed in overlapping aureoles. However, no definitive evidence of a rock affected by more than one metamorphic episode has been identified in the studied samples. The amount and mineralogy of the calc-silicate minerals that formed depend on the mineralogical composition of the protolith, especially regarding dolomite and silicate accessories (Fig. 11a, c). Orogenic compaction and deformation have obscured the width and shape configuration of the thermal metamorphic aureoles. However, some metamorphic isograds based on prograde calc-silicate mineral assemblages can be partially inferred (Figs. 3, 4, 5).

Calcite consistently appears as the predominant carbonate phase, with exceptions found in samples VCS-1 and BARB-15, where only minor dolomite is present. In the case of BARB-14, dolomite constitutes around 85% of the modal abundance and the samples VCS-4, MONF-9 and VLA-3B exhibit significant dolomite within the overall carbonate fraction.

Rocks containing calc-silicate minerals that were sampled far from the intrusions exhibit the typical mineral assemblages of the albite–epidote facies and appear to represent the lowest metamorphic grade. These include samples MONF-9 (with talc and epidote) and MONF-4, VCS-4 and VLA-1 (with tremolite), likely the product of low-grade contact metamorphism, translated by the first prograde metamorphic reactions in impure carbonates: dolomite (Dol) + quartz (Qz) + water (H_2O) = talc (Tlc) + calcite (Cal) + carbon dioxide (CO_2) followed by Tlc + Cal + Qz = tremolite (Trem) + H_2O + CO_2 when reaching the ca. 300–400 °C interval (Bucher 2023; Sharma and Sharma 2020; Winter 2014). The regular absence of talc

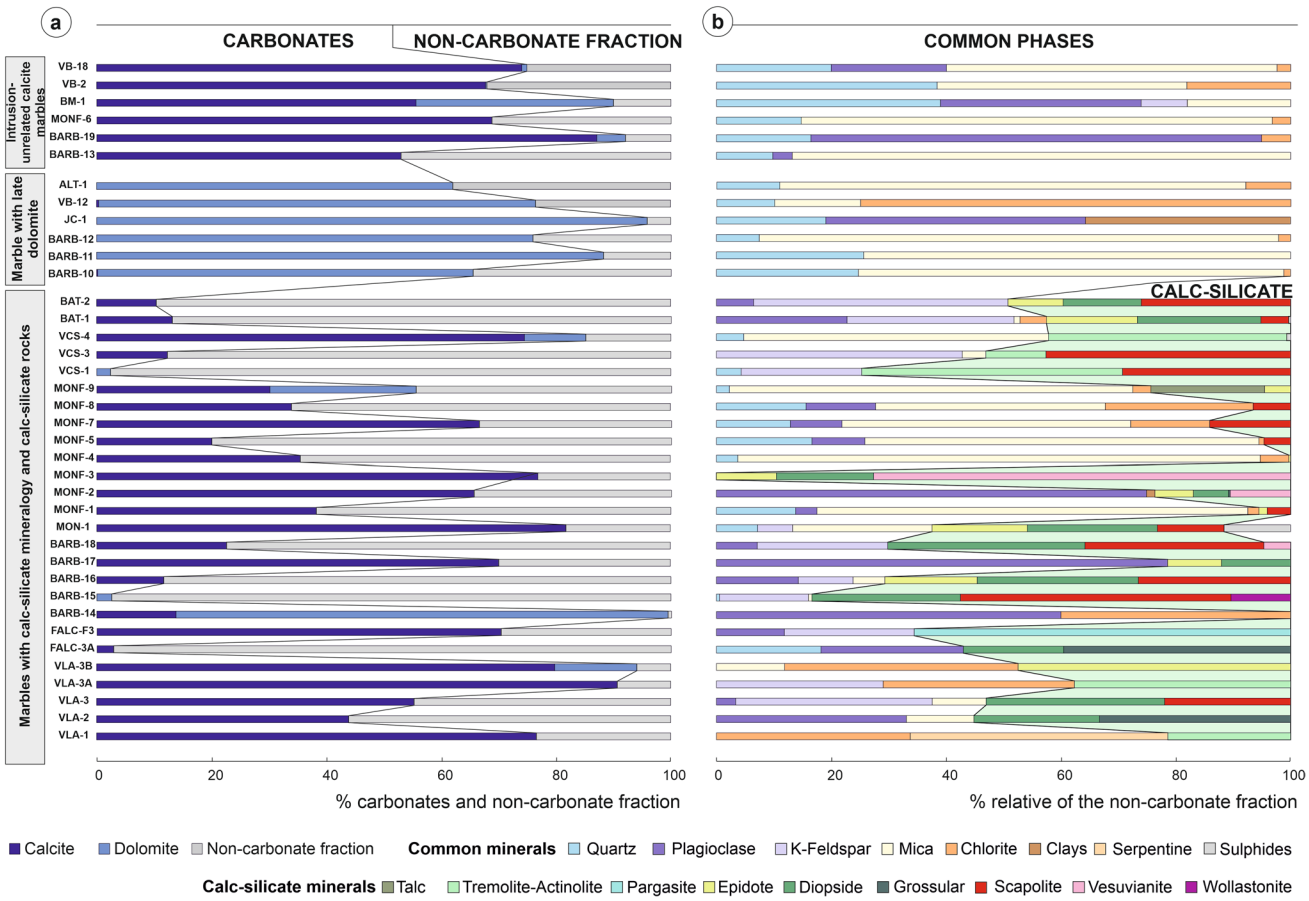

Fig. 8 **a** Results of x-ray diffraction (XRD) analysis for studied samples showing (**a**) the total abundance of calcite and dolomite in the rock and **b** the silicate mineralogy relative to the whole non-carbonate fraction, with fraction of silicates common to all groups and calc-silicate phases. Table of XDR data in Supplementary Information 1 (S1)

in the most external regions of the metamorphic aureole may be indicative of low water contents in the interstices or pore spaces of the protolith, leading to the direct formation of tremolite through $Dol + Qz + H_2O = Trem + Cal + CO_2$ (e.g., Sharma and Sharma 2020). The common presence of epidote can be explained by the reaction: plagioclase (Plg) + Cal + H_2O = epidote (Ep) + CO_2 (Winter 2014), implying the presence of detrital plagioclase in the protoliths. The prevalent calcite type I and type II twins in crystals from the albite–epidote samples seem compatible with the low-grade metamorphic conditions.

The occurrence of diopside may signify the establishment of medium-grade conditions (hornblende facies), resulting from temperatures reaching approximately 400–550 °C, at the expense of lower-grade assemblages, i.e., Trem + Cal + Qz = diopside (Di) + CO_2 + H_2O (Bucher 2023; Sharma and Sharma 2020). Diopside is found associated with all intrusions except the Vaiamonte massif. In the Falcato metamorphic aureole (sample FALC-F3) pargasite appears along with calcic amphiboles that show some replacement of calcium by sodium. These likely formed from lower temperature tremolites (e.g., Bucher 2023).

Medium grade rocks from roof pendants and enclaves exhibit diopside, vesuvianite (in the SEPC, samples MONF-3 and MONF-2) and garnet (predominantly in northern Falcato and Almendral, in samples FALC-3A and VLA-2). Vesuvianite can occur at lower temperatures (e.g., Winkler 1976) however, the typical association with diopside in studied samples suggest it was formed at least at medium grade conditions (samples MONF-2, MONF-3 and BARB-18). In the Almendral roof pendant, anisotropic garnet is assumed to be hydrogrossular (OH^-bearing garnet, Rossman and Aines 1991), characterized by concentric zonation or atolls surrounding calcite or epidote, implying retrogression (Fig. 7g).

Garnets can be produced either at the expense of common protolith minerals via Cal + Plg + Qz = garnet (Grt) + CO_2, or through the prograde reaction Ep + Cal + Qz = Grt + H_2O (Bucher 2023; Sharma and Sharma 2020). Fluorite was only found in a calcite-epidote vein in the medium-grade Almendral roof pendant (near VLA-2) possibly resulting from

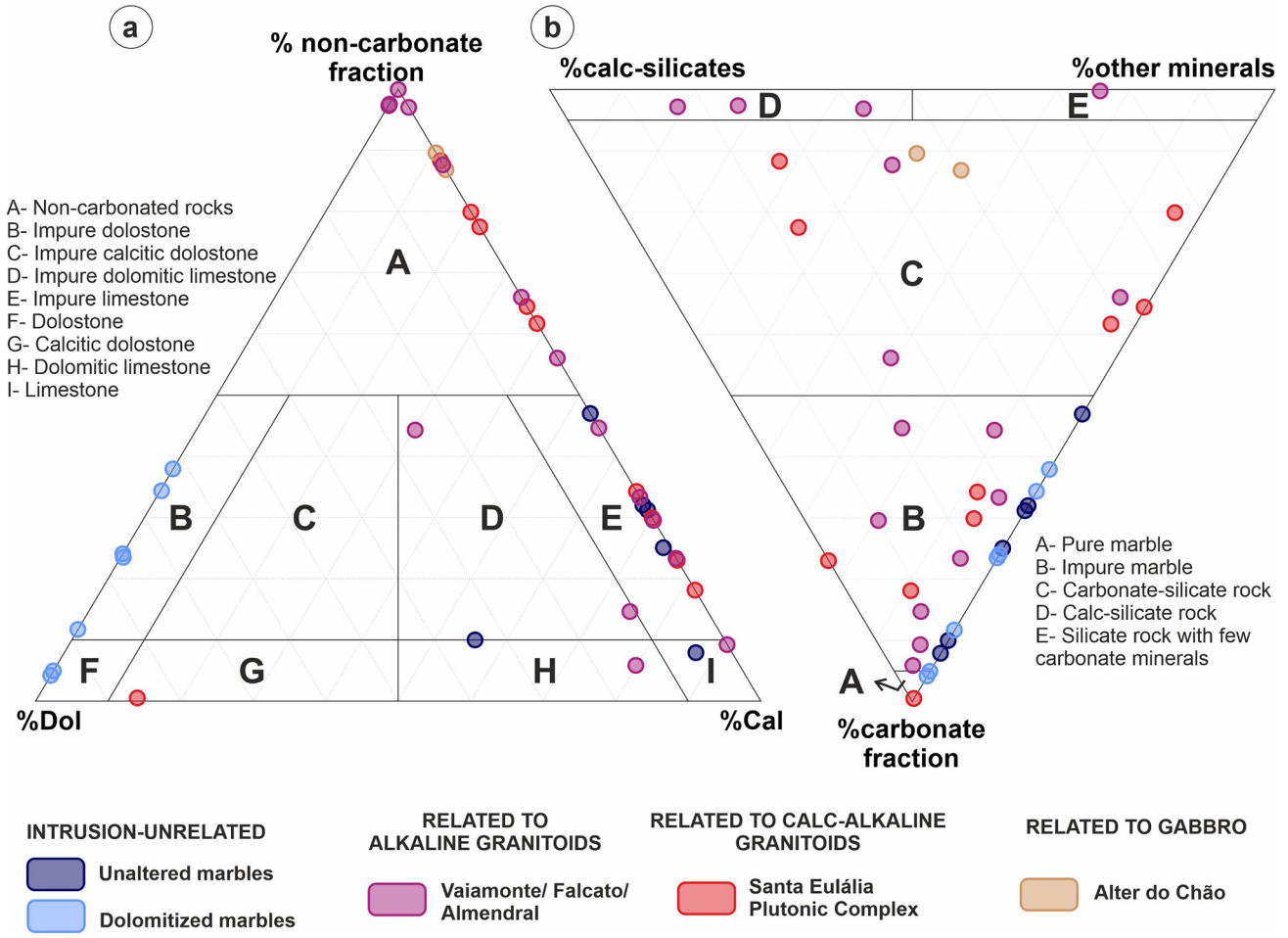

Fig. 9 Ternary diagrams of mineralogical composition plotting obtained XRD results. **a** Applying the sedimentary rock nomenclature according to carbonate fraction (from Giannini 2003). **b** Distinguishing impure marbles and rocks bearing calc-silicate minerals (adapted from Davis and Ferry 1993; Mathieu et al. 2015). Carbonate fraction represents the percentage of calcite (%Cal) and dolomite (%Dol) in each sample. Minerals comprising the modal abundance of other minerals and calc-silicate minerals as in Fig. 8

the action of fluids expelled from the alkaline-peralkaline intrusion.

At medium-grade conditions, calcite becomes less common (expected since most metamorphic reactions imply decarbonization). Calcite in these samples is usually not twinned or shows type IV twins (Fig. 7j) which develop at higher temperatures than calcite with type I and type II twins.

In the inner belts of the thermal aureoles, higher grade samples (ca. 550–700 °C) consistently contain scapolite, presumably formed through the reaction Plg + Cal = scapolite (Scp) (Bucher 2023; Sharma and Sharma 2020). Scapolite was observed near all intrusions except near the Falcato massif. Even though wollastonite has not been confirmed in thin section, its presence in a SEPC roof pendant (BARB-15) is not unreasonable, as the simple reaction Cal + Qz = wollastonite (Wo) + CO_2 can happen at high temperatures (e.g., Bucher 2023).

No forsterite was present in any of the collected semples. This could be due to the protolith composition, as the presence of forsterite in metamorphosed silicious dolostones is favored if the protolith contains high Mg/Fe and low SiO_2, whereas low Mg/Fe and high SiO_2 favors the appearance of diopside (Winter 2014). Similar reasons could explain the absence of periclase, since this mineral is only expected in rocks derived from SiO_2-poor and (Al_2O_3-poor) dolostones or dolomitic limestones (e.g., Bucher 2023).

The occurrence of garnet, vesuvianite, fluorite and wollastonite appear to be restricted to the roof pendants, which suggests that the external fluid flow and thermal dispersion is heterogenous around the intrusions. Jamtveit et al. (1992) and Winter (2014) suggest that the occurrence of wollastonite- and garnet-in reactions are triggered by H_2O-rich intrusion-driven reaction fronts near magmatic bodies, as they require a CO_2-poor fluid. In addition, Winter (2014) also suggested that the formation of vesuvianite is associated

Table 2 Results of $^{87}Sr/^{86}Sr$ analysis for the studied samples

	Sample	$^{86}Sr/^{87}Sr$	Error (2σ)
Not related to intrusions			
Calcite low-grade marbles			
Outeirão	BM-1	0.708315	0.000031
Vila Boim	VB-2*	0.708777	0.000013
Vila Boim	VB-18*	0.708538	0.000021
Monforte	MONF-6	0.708493	0.000021
Barbacena	BARB-13	0.708480	0.000027
Barbacena	BARB-19	0.708481	0.000023
Late dolomitized rocks			
Alter do Chão	ALT-1*	0.709227	0.000024
Vila Boim	VB-12*	0.709136	0.000030
Jerez de los Caballeros	JC-1	0.709250	0.000028
Barbacena	BARB-10	0.709478	0.000021
	BARB-11**	0.709546	0.000023
	BARB-12	0.708964	0.000018
Related to intrusions			
Related to alkaline-peralkaline rocks			
Falcato	FALC-3A	–	–
	FALC-F3	0.708758	0.000023
Vaiamonte (NW)	VCS-1	–	–
	VCS-3	0.709106	0.000026
	VCS-4	0.708146	0.000028
Vaiamonte (SE)	MONF-7	0.708944	0.000020
	MONF-8	0.709586	0.000018
	MONF-9	0.708542	0.000020
Almendral	VLA-1	0.708760	0.000026
	VLA-2	0.709531	0.000018
	VLA-3	0.708689	0.000018
	VLA-3A	0.708378	0.000028
	VLA-3B	0.708412	0.000027
Related to gabbroic rocks			
Alter do Chão	BAT-1	0.709393	0.000021
	BAT-2	0.709061	0.000020
Related to calc-alkaline granitoids			
Santa Eulália Plutonic Complex	MONF-1	0.708692	0.000018
	MONF-4	0.708526	0.000027
	MONF-5	0.708764	0.000023
	BARB-14	0.708359	0.000018
	BARB-18	0.709434	0.000017
	MON-1	0.708498	0.000021
	MONF-2	0.708515	0.000024
	MONF-3	0.708573	0.000021
	BARB-15	–	–
	BARB-16	0.708781	0.000024
	BARB-17	0.708459	0.000023

*Previously published by Moreira et al. (2019)

with water-rich fluids. In this way, the presence of such mineralogy in roof pendants and enclaves could be explained by the preference for intrusion-derived fluid pathways, leading to high-H_2O ingress into the country rocks above the intrusion, since the upwards route through hydraulic fractures and faults would be the most likely path, due to the low density of the aqueous fluids. In contrast, the sideways movements of intrusion-related fluids depend largely on the porosity, permeability and structure (e.g., bedding planes or foliation). This could explain the mineralogy typical of internally buffered reactions (precursor minerals reacting with pore fluids to maintain a relatively stable chemical composition despite temperature changes) found around the intrusive bodies since the massive character of the original marls and limestones of the Carbonate Formation (e.g., Araújo et al. 2013) would have prevented sideways fluid circulation. Table 3 summarizes the sample distribution regarding the thermal metamorphic grades of the studied samples.

The origin of mica, plagioclase and K-feldspar in the studied calc-silicate rocks (s.l.) is still uncertain, as these minerals can be either inherited (detrital) and therefore stable under a wide thermal range (as discussed in Moreira et al. 2019) or a product of metamorphic recrystallization. Major retrogression features consist of garnet breakdown to epidote, quartz and calcite (Fig. 7g, i–j) and, less commonly, scapolite to plagioclase, calcite and epidote. These observed retrogression features could suggest the breakdown of high-grade minerals during later regional greenschist facies metamorphism, thermal relaxation during exhumation or decompression.

Implications of mineralogical modifications on the Sr-Isotopic signature

The $^{87}Sr/^{86}Sr$ values obtained for the carbonate fraction of the calc-silicate rocks with low-grade metamorphic assemblages are compatible with the signature of regional marbles not related with intrusions ($^{87}Sr/^{86}Sr < 0.7088$). Dolomite is unstable at the temperatures of the higher albite–epidote facies and the calc-silicate mineral assemblages are mainly produced with total consumption of dolomite, usually forming residual hydrothermal calcite (Sharma and Sharma 2020). This could be due to internal buffering being able to preserve the previous $^{87}Sr/^{86}Sr$ composition. The heat transferred by conduction from the igneous body would vaporize interstitial waters in massive limestones, which inhibit pervasive fluid flow. Vaporization would promote local reactions without substantial Sr influx, thus maintaining the precursor Sr isotopic signature. Despite that, high-grade rocks located near the intrusion with significant amounts of calc-silicates (>25%) show an increase in $^{87}Sr/^{86}Sr$ values that slightly contrast with the typical signature of unaltered

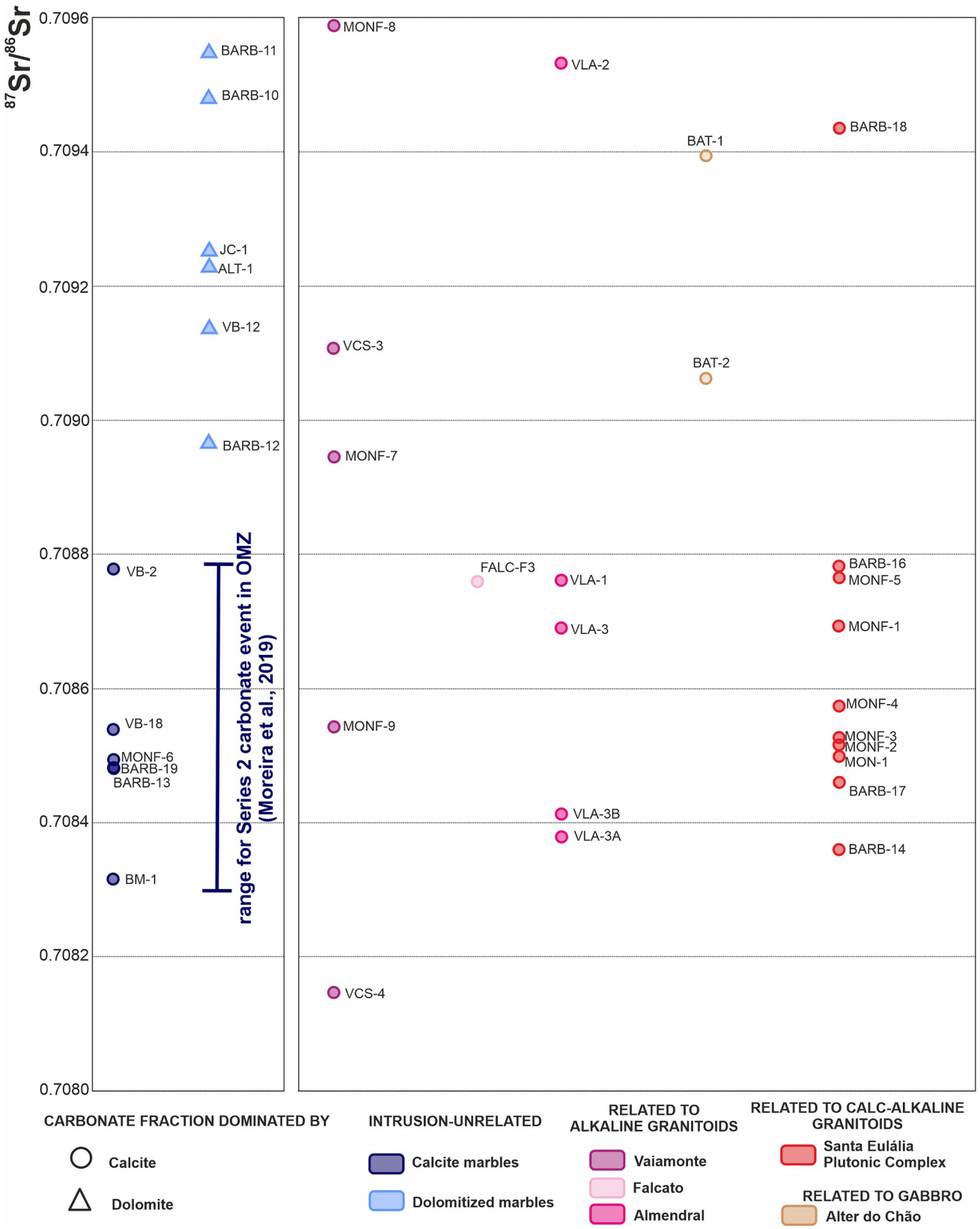

Fig. 10 $^{87}Sr/^{86}Sr$ from marbles and dolostones collected distally from and proximally from igneous bodies. $^{87}Sr/^{86}Sr$ from carbonate rocks from other OMZ locations are plotted for comparison (from Moreira et al. 2019)

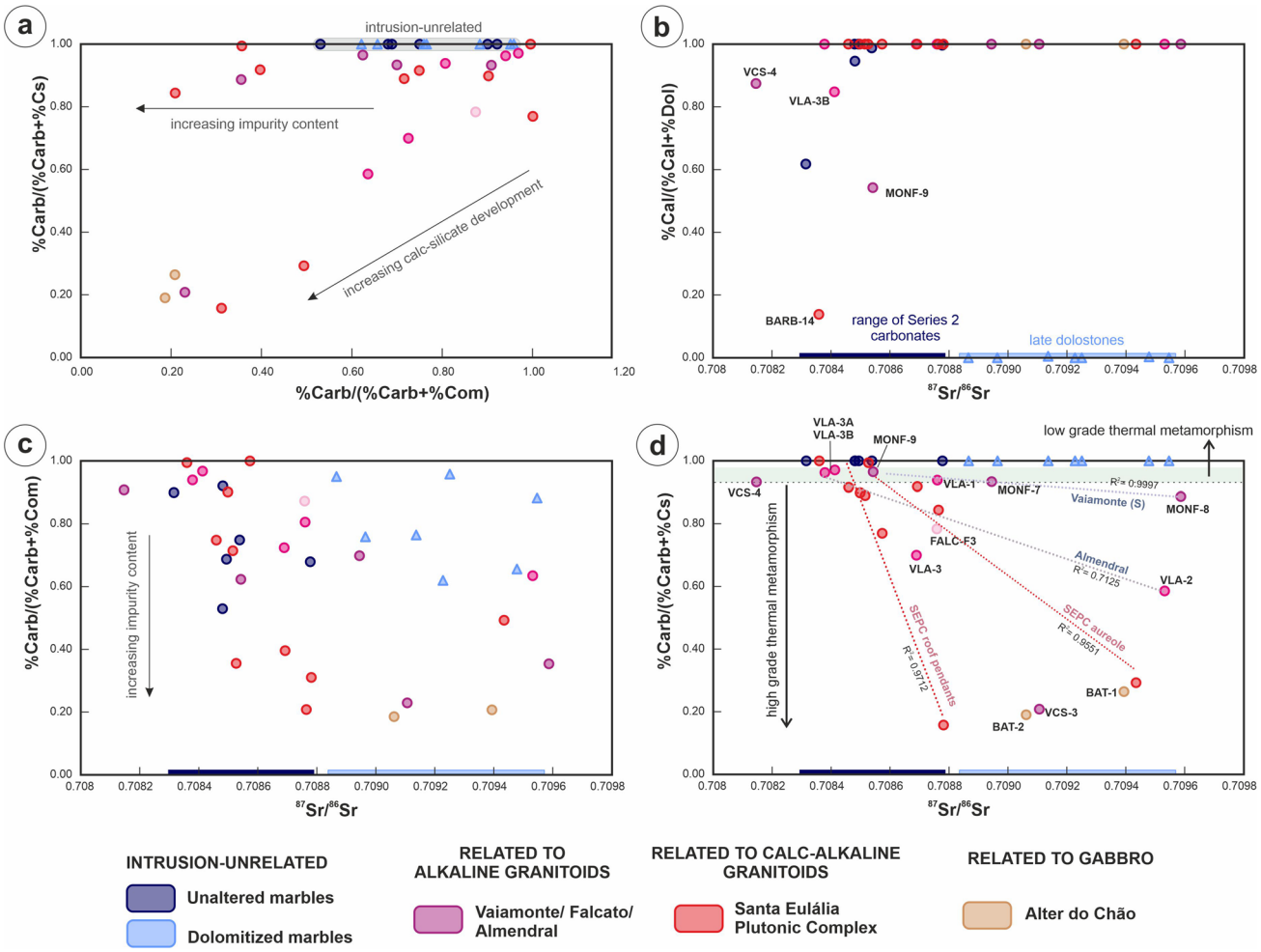

Fig. 11 Binary plots variation of mineralogical and $^{87}Sr/^{86}Sr$ values for all samples analyzed. **a** %Carb/(%Carb + %Com) vs %Carb/(%Carb + %Cs). **b** $^{87}Sr/^{86}Sr$ values vs the carbonates ratio. **c** $^{87}Sr/^{86}Sr$ values vs %Carb/(%Carb + %Com). **d** $^{87}Sr/^{86}Sr$ values vs %Carb/(%Carb + %Cs). %Carb refers to the modal abundance of calcite and dolomite, %Cal and %Dol refer to calcite and dolomite respectively, %Com encompasses the common mineralogy excluding the calc-silicate phases and %Cs the amount of calc-silicate mineralogy

Table 3 Summary of thermal grades according to the calc-silicate phases and calcite (Cc) twin types found on samples from the Carbonate Formation of the OMZ, with information on their location within the aureole configuration (near the outer, middle, or inner isograds) and position relative to the intrusion (on the sideways of the magmatic bodies or in enclaves as roof pendants)

Facies	Calc-silicate phase	Cc Twin	Sample	Isograd	Location
Albite–epidote	Epidote	I, II	MONF-9	Out	Side
	Tremolite	I, II, IV	VCS-4, MONF-4	Out	Side
T (°C) = 300–400	Tremolite	I, II	VLA-1	Out	Enclave
Hornblende	Garnet (grossular)	I, II, III, IV	FALC-3A, VLA-2	Mid	Enclave
T (°C) = 400–550	Vesuvianite	I, II, IV	MONF-2, MONF-3*	Mid	Enclave
Pyroxene	Scapolite (w/ diopside)	I, II, IV	BAT-1, BAT-2, VCS-1, VCS-3, BARB-18, MONF-1, MONF-5, MONF-7, MONF-8	In	Side
	Scapolite	I, II, IV	VLA-3, MON-1, BARB-16 BARB-17	In	Enclave
T (°C) = 500–700	Wollastonite	–	BARB-15	In	Enclave

Samples with no calc-silicate minerals are not presented

Cambrian marbles (Figs. 9, 11d). Although the lack of detailed results for each individual area of sample collection, a plot of the regional data shows a wide fan-shaped pattern, suggesting a non-linear relationship between the development of calc-silicate minerals and the increase of the radiogenic Sr isotopic signature in carbonates (Fig. 11d). Samples with higher grade assemblages (BAT-1, BAT-2 and FALC-F3) fall within the pattern (Fig. 11d).

The non-carbonate mineral fraction in the protolith appears to exert a strongcontrol on the formation of the thermal metamorphic mineral assemblages. Sample BARB-14, located in the vicinity of the SEPC calc-alkaline granitoid, is composed almost exclusively of carbonates and displays the established Cambrian $^{87}Sr/^{86}Sr$ signature. This observation provides further evidence of carbonate recrystallization buffering the Sr values in samples that did not develop calc-silicate minerals. Samples VLA-3A and VLA-3B (also collected near an intrusion, in the Almendral roof pendant) similarly confirm such inferences, with poor development of calc-silicate phases and maintenance of the protolith $^{87}Sr/^{86}Sr$ values. This could be due to no quartz being present in the assemblages, hindering the progression of the thermal reactions. Rocks in the outer thermal aureole (VCS-4, MONF-4, MONF-9, VLA-1) that did not pass albite–epidote conditions, did not undergo the further metamorphic reactions that promote decarbonation, and therefore were also able to preserve low $^{87}Sr/^{86}Sr$ values (Fig. 11d). Moreover, rocks with medium- to high-grade minerals fall within the fan-dispersion area, suggesting a link between the Sr signature and a decrease in the carbonate fraction (due to decarbonation reactions). The exact nature of the trends vary with the type of intrusion (Fig. 11d). The increase in $^{87}Sr/^{86}Sr$ with increasing grade could be due to external input of magmatic-derived Sr or to the successive decarbonation reactions of the rocks through the contact metamorphic stages. If both processes contributed to the thermal metamorphic overprint on the studied rocks, they would show significantly different trends.

Overall, the rocks metamorphosed at hornblende facies or higher that underwent mineralogical, or those that experienced dolomitization, pose a challenge for using Sr-based chronology (c.f. Moreira et al. 2019). However, Sr chronology systematics still appear to hold in samples where the metamorphic conditions did not pass the albite–epidote facies or in samples where the protolith is only composed of carbonate minerals. These types of samples generally preserve the initial $^{87}Sr/^{86}Sr$ ratios, thus maintaining their effectiveness for chronologic assessments.

Conclusions

The regionally metamorphosed Series 2 carbonate rocks of the OMZ include calcite or calcite–dolomite impure marbles and marlstones with accessory quartz, feldspars, mica and chlorite, and display $^{87}Sr/^{86}Sr$ values of 0.7083–0.7088, typical of lower Cambrian seawaters. Late dolomitization is characterized in samples that were unaffected by contact metamorphism by the growth of rhombohedral dolomite, with total replacement of calcite, and an increase in $^{87}Sr/^{86}Sr$ values >0.7088. Contact metamorphism in the ACECMu is characterized by a mineralogical and $^{87}Sr/^{86}Sr$ overprint in aureoles around intrusions. The main observations may be summarized as:

- The typical prograde assemblage preserved in the outer aureole is epidote + amphibole (usually tremolite), followed by the appearance of diopside in the middle aureole and by scapolite in the inner aureole. A fluid-driven transformation is suggested within the roof pendants and enclaves based on the almost exclusive presence of garnet (±fluorite), vesuvianite and wollastonite in rocks from these settings. In rocks with a high modal proportion of silicate minerals located near the igneous bodies (in the roof pendants, enclaves or adjacent to the intrusion), the primary carbonate minerals are substantially substituted by calc-silicate assemblages.
- The extent to which $^{87}Sr/^{86}Sr$ values in the carbonate fraction are modified by thermal metamorphism or retain the protolith signature is still unclear. Our results suggest that distance from the intrusion does not directly correlate to the carbonate $^{87}Sr/^{86}Sr$ ratio. Samples with a higher abundance of silicate minerals were likely more reactive during thermal perturbations, leading to changes in mineralogy and hence isotopic signatures with increasing decarbonization at higher temperature. The $^{87}Sr/^{86}Sr$ ratio in carbonate phases tends to increase with the growth of calc-silicate mineral assemblages and decreasing carbonate modal proportion) above hornblende-facies conditions. These conditions therefore provide a limit to carbonate Sr-isotope chronology. The exception provided by marbles with a very high carbonate fraction located adjacent to the intrusions. These remained unreactive during contact metamorphism and consequently they maintain their Cambrian strontium isotope fingerprint.

Supplementary Information The online version contains supplementary material available at https://doi.org/10.1007/s00531-024-02476-w.

Acknowledgements The authors are grateful for the careful reviews by Ícaro Dias da Silva and Rubén Díez Fernández, which provided many insightful comments and constructive suggestions that deeply improved the quality of the manuscript. We are also extremely thankful to Clare

Warren for the kind and careful revisions that profoundly refined the final version of this work. The suggestions and editorial handling from Ulrich Riller are likewise truly acknowledged. Sandra Velez is thanked for all the support during the methodological processes in the laboratories of the Department of Geosciences of the University of Évora, specifically for the preparation of thin sections and pulps. J. Roseiro acknowledges Fundação para a Ciência e Tecnologia, I.P. (FCT), for support through the doctoral grant with reference UI/BD/150937/2021 (https://doi.org/10.54499/UI/BD/150937/2021), and to the Society of Economic Geologists for funding through the Hugh McKinstry Fund (SRG 21-46 award). J. Roseiro, N. Moreira and P. Nogueira acknowledge the support granted to Instituto das Ciências da Terra through the FCT projects: UIDB/04683/2020 and UIDP/04683/2020 (https://doi.org/10.54499/UIDB/04683/2020 and https://doi.org/10.54499/UIDP/04683/2020 respectively). Analyses conducted in the HERCULES laboratory of the University of Évora were supported by FCT through UIDB/04449/2020 and UIDP/04449/2020. Isotope analyses, carried out at the Laboratory of Isotope Geology of the University of Aveiro, were funded by FCT, through GeoBioTec (UIDB/04035/2020). Some results presented here were partially funded through project ZOM3D (Modelos Metalogénicos 3D da Zona de Ossa-Morena—Valorização dos Recursos Minerais do Alentejo), with reference ALT20-03-0145-FEDER-000028, funded by Alentejo 2020 (Regional Operational Program of Alentejo) through the FEDER/FSE/FEEI programmes.

Authors contributions Conceptualization**:** J. Roseiro; N. Moreira Methodology: J. Roseiro, N. Moreira, J. Pedro formal analysis and investigation**:** J. Roseiro, L. Andrade, N. Moreira, P. Moita, J. Francisco Santos, S. Ribeiro writing—original draft preparation: J. Roseiro, Noel Moreira writing—review and editing**:** All authors Funding Acquisition: N. Moreira, J. Pedro; P. Nogueira, J. Mirão, J. Francisco Santos Supervision: N. Moreira, P. Nogueira, D. de Oliveira, J. Pedro, L Eguiluz.

Funding Open access funding provided by FCT|FCCN (b-on).

Data availability Data is all in the tables along the text and in the supplementary material.

Declarations

Conflict of interest The authors declare no competing interests relevant to the content of this article.

References

Álvaro JJ, Bellido F, Gasquet D, Pereira MF, Quesada C, Sánchez-García T (2014) Diachronism in the late Neoproterozoic-Cambrian arc-rift transition of North Gondwana: a comparison of Morocco and the Iberian Ossa-Morena Zone. J Afr Earth Sci 98:113–132. https://doi.org/10.1016/j.jafrearsci.2014.03.024

Andrade L (2022) Caracterização mineralógica e isotópica das rochas carbonatadas no setor de Alter do Chão—Elvas (zona de Ossa Morena). Unpublished MSc Thesis, University of Évora, p 81. http://hdl.handle.net/10174/31410

Armendáriz M (2006) Los depósitos carbonatados de la cuenca carbonífera del Guadiato (Córdoba, SO del Macizo Ibérico). Bol Geol Min 117:513–518

Araújo A, Piçarra de Almeida J, Borrego J, Pedro J, Oliveira T (2013) As regiões central e sul da Zona de Ossa-Morena. In: Dias R, Araújo A, Terrinha P, Kullberg JC (eds) Geologia de Portugal, Volume 1. Escolar Editora, pp 509–549

Ayan T (1965) Chemical staining methods used in the identification of carbonate minerals. BMRE 65:10

Bucher K (2023) Petrogenesis of metamorphic rocks. Springer Nature, p 467

Cambeses A, Molina JF, Morales I, Lázaro C, Moreno JA, Montero P, Bea F (2021) Compositional evolution of the Variscan intra-orogenic extensional magmatism in the Valencia del Ventoso Plutonic Complex, Ossa-Morena Zone (SW Iberia): a view from amphibole compositional relationships. Minerals 11(4):431. https://doi.org/10.3390/min11040431

Cambeses A, Montero P, Molina JF, Hyppolito T, Bea F (2019) Constraints of mantle and crustal sources and interaction during orogenesis: a zircon SHRIMP U-Th-Pb and O isotope study of the "calc-alkaline" Brovales pluton, Ossa-Morena Zone, Iberian Variscan Belt. Lithos 324–325:661–683. https://doi.org/10.1016/j.lithos.2018.11.037

Cambeses A, Scarrow JH, Montero P, Molina JF, Moreno JA (2015) SHRIMP U-Pb zircon dating of the Valencia del Ventoso plutonic complex, Ossa-Morena Zone, SW Iberia: early carboniferous intra-orogenic extension-related 'calc-alkaline' magmatism. Gondwana Res 28(2):735–756. https://doi.org/10.1016/j.gr.2014.05.013

Carriedo J, Tornos F, Velasco F, Terrón A (2006) Mineralizaciones de magnetita asociadas a skarns y bandas de cizalla: La mina de Cala (Huelva). Geogaceta 40:235–238

Carrilho Lopes J (2020) Magmatismo Intrusivo no Ciclo Varisco. University ff Évora, p 566

Chichorro MAFDS (2006) A evolução tectónica da zona de cisalhamento de Montemor-o-Novo (sudoeste da zona de Ossa Morena-área de Santiago do Escoural-Cabrela). Unpublished PhD Thesis, University of Évora, p 521

Chichorro M, Pereira MF, Diaz-Azpiroz M, Williams IS, Fernández C, Pin C, Silva JB (2008) Cambrian ensialic rift-related magmatism in the Ossa-Morena Zone (Évora–Aracena metamorphic belt, SW Iberian Massif): Sm–Nd isotopes and SHRIMP zircon U–Th–Pb geochronology. Tectonophysics 461(1–4):91–113. https://doi.org/10.1016/j.tecto.2008.01.008

Cózar P, Somerville ID, Rodríguez S, Mas R, Medina-Varea P (2006) Development of a late Viséan (Mississippian) mixed carbonate/siliciclastic platform in the Guadalmellato Valley (southwestern Spain). Sed Geol 183(3–4):269–295. https://doi.org/10.1016/j.sedgeo.2005.09.018

Cruz C (2013) Efeitos metamórficos e fluidos do Complexo Plutónico de Santa Eulália. Unpublished MSc Thesis, University of Porto, p 92

Cruz C, Roseiro J, Martins HCB, Nogueira P, Noronha F, Sant'Ovaia H (2022) Magmatic sources and emplacement mechanisms of the Santa Eulália Plutonic Complex facies: integrating geochronological and geochemical data. XIII Congreso Nacional y XIII Ibérico de Geoquímica, pp 223–230

Dallmeyer RD, García-Casquero JL, Quesada C (1995) 40Ar/39Armineral age constraints on the emplacement of the Burguillos del Cerro Igneous complex (Ossa-Morena zone, SW Iberia). Bol Geol Min 106:203–214

Davis SR, Ferry JM (1993) Fluid infiltration during contact metamorphism of interbedded marble and calc-silicate hornfels, Twin Lakes area, central Sierra Nevada, California. J Metamorph Geol 11(1):71–88. https://doi.org/10.1111/j.1525-1314.1993.tb00132.x

Denison RE, Koepnick RB, Burke WH, Hetherington EA, Fletcher A (1997) Construction of the Silurian and Devonian seawater 87Sr/86Sr curve. Chem Geol 140:109–121. https://doi.org/10.1016/S0009-2541(97)00014-4

Dias G, Simões PP, Ferreira N, Leterrier J (2002) Mantle and crustal sources in the genesis of Late-Hercynian granitoids (NW Portugal): geochemical and Sr-Nd isotopic constraints. Gondwana Res 5:287–305. https://doi.org/10.1016/S1342-937X(05)70724-3

Dias da Silva Í, Pereira MF, Clavijo EG, Silva JB (2024) Mississippian olistostromes of Iberia revisited: tectonic drivers of synorogenic carbonate platform/reef destruction. JGS 181(2):jgs2023-187. https://doi.org/10.1144/jgs2023-187

Dias da Silva Í, Pereira MF, Gama C, Steel Hart L, Barrios Sánchez S, dos Santos Alves K, Gómez Barreiro J, Tassinari CCG, Sato K (2023) The influence of synorogenic extension on the crustal architecture of North Gondwana during the assembly of Pangaea (Ossa–Morena Zone, SW Iberia). GSL SP 542(1):SP542-2023.10.1144/sp542-2023-9

Dias da Silva Í, Pereira MF, Silva JB, Gama C (2018) Time-space distribution of silicic plutonism in a gneiss dome of the Iberian Variscan Belt: the Évora Massif (Ossa-Morena Zone, Portugal). Tectonophysics 747:298–317. https://doi.org/10.1016/j.tecto.2018.10.015

Díez Fernández R, Pereira MF, Foster DA (2015) Peralkaline and alkaline magmatism of the Ossa-Morena zone (SW Iberia): age, source, and implications for the Paleozoic evolution of Gondwanan lithosphere. Lithosphere 7(1):73–90. https://doi.org/10.1130/L379.1

Errandonea-Martin J, Sarrionandia F, de Madinabeitia SG, Beranoaguirre A, Carracedo-Sánchez M, Garate-Olave I, Ibarguchi JIG (2024) Geochemical evidence for crustal anatexis during intraorogenic transcurrent tectonics: insights from Variscan peraluminous granites from the La Bazana Pluton (Ossa–Morena Zone, Iberian Massif). Lithos 472:107555. https://doi.org/10.1016/j.lithos.2024.107555

Etxebarria M, Chalot-Prat F, Apraiz A, Eguíluz L (2006) Birth of a volcanic passive margin in Cambrian time: rift paleogeography of the Ossa-Morena Zone, SW Spain. Precambrian Res 147(3–4):366–386. https://doi.org/10.1016/j.precamres.2006.01.022

Expósito I, Simancas JF, González Lodeiro F, Bea F, Montero P, Salman K (2003) Metamorphic and deformational imprint of Cambrian-Lower Ordovician rifting in the Ossa-Morena Zone (Iberian Massif, Spain). J Structural Geol 25:2077–2087. https://doi.org/10.1016/s0191-8141(03)00075-0

Faure G, Mensing TM (2005) Isotopes. Principles and applications. Wiley, p 897

Giannini PCF (2003) Depósitos e rochas sedimentares. In: Texeira W, Toledo MCM, Fairchild TR, Taioli F (eds) Decifrando a Terra. São Paulo, Oficina de Textos, pp 285–304

Gonçalves F (1971) Subsídios para o conhecimento geológico do Nordeste Alentejano. Serviços Geológicos de Portugal. Memória nº 18, p 62

Gonçalves F, Assunção CT (1970) Carta geológica de Portugal na escala de 1: 50 000: notícia explicativa da folha 37-A: Elvas

Gonçalves F, Fernandes AP (1973) Carta geológica de Portugal na escala de 1: 50 000: notícia explicativa da folha 32-B: Portalegre

González MP, Palacios T, Valenzuela JG (1990) Trilobites y goniatites de la cuenca carbonífera de los Santos de Maimona: deducciones bioestratigráficas. Geogaceta 8:66–67

Gozalo R, Liñán E, Palacios T, Gámez-Vintaned JA, Mayoral E (2003) The Cambrian of the Iberian Peninsula: an overview. Geol Acta 1:103–112

Gutiérrez-Marco JC, Piçarra JM, Meireles CA, Cózar P, García-Bellido DC, Pereira Z, Vaz N, Pereira S, Lopes G, Oliveira JT, Quesada C, Zamora S, Esteve J, Colmenar J, Bernardéz E, Coronado I, Lorenzo S, Sá AA, Dias da Silva Í, González-Clavijo E, Díez-Montes A, Gómez-Barreiro J (2019) Early Ordovician–Devonian Passive Margin Stage in the Gondwanan Units of the Iberian Massif. In: Quesada C, Oliveira JT (eds) The geology of Iberia: a geodynamic approach. Vol.2: the Variscan cycle. Springer (Berlin), Regional Geology Series, pp 75–98 https://doi.org/10.1007/978-3-030-10519-8_3

Hubbard CR, Evans EH, Smith DK (1976) The reference intensity ratio, I/Ic, for computer simulated powder patterns. J Appl Cryst 9(2):169–174. https://doi.org/10.1107/S0021889876010807

Hubbard CR, Snyder RL (1988) RIR-measurement and use in quantitative XRD. Powder Diffr 3(2):74–77. https://doi.org/10.1017/S0885715600013257

Jamtveit B, Grorud HF, Bucher-Nurminen K (1992) Contact metamorphism of layered carbonate-shale sequences in the Oslo Rift. II: Migration of isotopic and reaction fronts around cooling plutons. Earth Planet Sci Lett 114(1):131–148. https://doi.org/10.1016/0012-821X(92)90156-P

Jesus AP, Mateus A, Munhá JM, Tassinari CC, dos Santos TMB, Benoit M (2016) Evidence for underplating in the genesis of the Variscan synorogenic Beja Layered Gabbroic Sequence (Portugal) and related mesocratic rocks. Tectonophysics 683:148–171. https://doi.org/10.1016/j.tecto.2016.06.001

Jesus AP, Munhá J, Mateus A, Tassinari C, Nutman AP (2007) The Beja Layered Gabbroic Sequence (Ossa-Morena Zone, Southern Portugal): geochronology and geodynamic implications. Geodin Acta 20:139–215. https://doi.org/10.3166/ga.20.139-157

Julivert M, Fontboté JM, Ribeiro A, Conde L (1974) Mapa Tectónico de la Península Ibérica y Baleares. Escala 1: 1,000,000. Memoria Explicativa. Instituto Geológico y Minero de España, Madrid, p 113

Lains Amaral J, Mata J, Santos JF (2022) The carboniferous shoshonitic (s.l.) gabbro-monzonitic stocks of Veiros and Vale de Maceira, Ossa-Morena Zone (SW Iberian Massif): Evidence for diverse subduction-related lithospheric metasomatism. Geochemistry 82(4):125917. https://doi.org/10.1016/j.chemer.2022.125917

Liñán E, Perejón A, Gozalo R, Moreno-Eiris E, Oliveira TJ (2004) The Cambrian system in Iberia. Cuadernos del Museo Geominero No 3, Instituto Geológico y Minero de España, Madrid, p 63

Lotze F (1945) Zur gliederung der Varisziden der Iberischen meseta. Geoteckt Forsch 6:78–92

Machado G, Hladil J, Koptikova L, Fonseca P, Rocha FT, Galle A (2009) The Odivelas limestone: evidence for a middle Devonian reef system in western Ossa-Morena zone. Geol Carpath 60(2):121–137. https://doi.org/10.2478/v10096-009-0008-1

Machado G, Hladil J, Koptikova L, Slavik L, Moreira N, Fonseca M, Fonseca P (2010) An Emsian-Eifelian carbonate-volcaniclastic sequence and the possible record of the basal choteč event in western Ossa-Morena zone, Portugal (Odivelas Limestone). Geol Belg 13:431–446

Machado G, Moreira N, Silvério G (2020) Devonian Sedimentation in the SW boundary of the Ossa-Morena zone: state of art and paleogeography. Com Geol 107(I):43–47

Maia M, Barrulas P, Nogueira P, Mirão J, Noronha F (2022) In situ LA-ICP-MS trace element analysis of magnetite as a vector towards mineral exploration: a comparative case study of Fe-skarn deposits from SW Iberia (Ossa-Morena Zone). J Geochem Explor 234:106941. https://doi.org/10.1016/j.gexplo.2021.106941

Mata J, Munhá J (1990) Magmatogénese de metavulcanitos Câmbricos do Nordeste Alentejano: Os estádios iniciais de rifting continental. Comun Serv Geol 76:61–89

Mathieu L, Trépanier S, Daigneault R (2015) CONSONORM_HG: a new method of norm calculation for mid-to high-grade metamorphic rocks. J Metamorph Geol 34(1):1–15. https://doi.org/10.1111/jmg.12168

Montero P, Salman K, Zinger T, Bea F (1999) Rb-Sr and single-zircon grain 207 Pb/206 Pb chronology of the Monesterio granodiorite and related migmatites. Evidence of a Late Cambrian melting event in the Ossa-Morena Zone, Iberian Massif. Estudios geológicos, 55(1–2):3–8

Moreira N (2017) Evolução Geodinâmica dos sectores setentrionais da Zona de Ossa-Morena no contexto do Varisco Ibérico. Unpublished PhD Thesis, University of Évora, p 433

Moreira N, Machado G, Fonseca PE, Silva JC, Jorge RCGS, Mata J (2010) The Odivelas Palaeozoic volcano-sedimentary sequence: implications for the geology of the Ossa-Morena Southwestern border. Comum Geol 97(1):129–146

Moreira N, Pedro JC, Santos J, Inês N, Araújo A, Dias R, Ribeiro S, Romão J, Mirão J (2018) Effects of secondary late dolomitization on 87Sr/86Sr isotopic ratio; examples from Ossa-Morena Zone carbonates. Abstract book of XIV Congresso de Geoquímica dos Países de Língua Portuguesa, XIX Semana da Geoquímica, pp 223–226

Moreira N, Pedro J, Santos JF, Araújo A, Dias R, Ribeiro S, Romão J, Mirão J (2019) 87Sr/86Sr applied to age discrimination of the Palaeozoic carbonates of the Ossa-Morena zone (SW Iberia Variscides). Int J Earth Sci 108(3):963–987. https://doi.org/10.1007/s00531-019-01688-9

Moreno-Martín D, Díez Fernández R, Arenas R, Rojo-Pérez E, Novo-Fernández I, Sánchez Martínez S (2023) Building and collapse of the cadomian orogen: a plate-scale model based on structural data from the SW Iberian Massif. Tectonics 42(12):e2023TC007990. https://doi.org/10.1029/2023TC007990

Muelas Peña A, Hernández Enrile JL, Solar Menéndez JB (1976) Mapa Geológico de España 1:50.000, hoja nº 827 (Alconchel) y memoria. IGME, p 30

Nance RD, Gutiérrez-Alonso G, Keppie JD, Linnemann U, Murphy JB, Quesada C, Strachan RA, Woodcock NH (2010) Evolution of the Rheic Ocean. Gondwana Res 17(2–3):194–222. https://doi.org/10.1016/j.gr.2009.08.001

Oliveira JT, González-Clavijo E, Alonso J, Armendáriz M, Bahamonde JR, Braid JA, Colmenero JR, Dias da Silva Í, Fernandes P, Fernández LP, Gabaldón V, Jorge RS, Machado G, Marcos A, Merino-Tomé Ó, Moreira N, Brendan Murphy J, Pinto de Jesus A, Quesada C, Rodrigues B, Rosales I, Sanz-López J, Suárez A, Villa E, Piçarra JM, Pereira Z (2019) Synorogenic basins. In: Quesada C, Oliveira JT (eds) The geology of Iberia: a geodynamic approach. Vol.2: the Variscan cycle, Regional Geology Series. Springer, Berlin, pp 349–429. https://doi.org/10.1007/978-3-030-10519-8_11

Oliveira JT, Oliveira V, Piçarra JM (1991) Traços gerais da evolução tectono-estratigráfica da Zona de Ossa-Morena. Cad Lab Xeol Laxe 16:221–250

Ochsner A (1993) U-Pb geochronology of the upper proterozoic–lower paleozoic geodynamic evolution in the Ossa-Morena Zone (SW Iberia): constraints on the timing of the Cadomian orogeny. Unpublished Ph.D. thesis, Zürich, ETH Zürich Unterstützen, 249 p

Ordóñez Casado B (1998) Geochronological studies of the pre-mesozoic basement of the Iberian Massif: the Ossa Morena Zone and the Allochthonous complexes within the Central Iberian Zone. Unpublished Ph.D. thesis, Zürich, Swiss Federal Institute of Technology, 235 p

Palacios T, Jensen S, Eguiluz L, Apalategui O, Martí M (2013) Mapa Geológico de Extremadura a escala 1:35.000. Servicio Editorial de la Universidad del País Vasco (UPV-EHU), Bilbao, p 222

Passchier CW, Trouw RA (2005) Microtectonics. Springer Science & Business, p 366

Pereira MF (1999) Caracterização da estrutura dos domínios setentrionais da Zona de Ossa-Morena e seu limite com a Zona Centro-Ibérica, no Nordeste Alentejano. Unpublished PhD thesis (Unpublished). Universidade de Évora, 114 pp

Pereira MP, Chichorro M, Williams IS, Silva JB, Fernández C, Díaz-Azpíroz M, Apraiz A, Castro A (2009) Variscan intra-orogenic extensional tectonics in the Ossa-Morena Zone (Évora–Aracena–Lora del Río metamorphic belt, SW Iberian Massif): SHRIMP zircon U–Th–Pb geochronology. Geolog Soc 327:215–237. https://doi.org/10.1144/SP327.11

Pereira MF, Chichorro M, Solá AR, Silva JB, Sánchez-García T, Bellido F (2011) Tracing the Cadomian magmatism with detrital/inherited zircon ages by in-situ U–Pb SHRIMP geochronology (Ossa-Morena Zone, SW Iberian Massif). Lithos 123(1–4):204–217. https://doi.org/10.1016/j.lithos.2010.11.008

Pereira MF, Dias da Silva Í, Rodríguez C, Corfu F, Castro A (2022) Visean high-K mafic-intermediate plutonic rocks of the Ossa-Morena Zone (SW Iberia): implications for regional extensional tectonics. Geolog Soc 531 (1):SP531-2022-2118. https://doi.org/10.1144/SP531-2022-118

Pereira MP, Gama C, Rodríguez C (2017) Coeval interaction between magmas of contrasting composition (Late Carboniferous-Early Permian Santa Eulália-Monforte massif, Ossa-Morena Zone): field relationships and geochronological constraints. Geola Acta 15(4):409–428. https://doi.org/10.1344/GeologicaActa2017.15.4.10

Pereira Z, Oliveira V, Oliveira JT (2006) Palynostratigraphy of the Toca da Moura and Cabrela Complexes, Ossa Morena zone, Portugal. Geodynamic implications. Rev Palaeobot Palyno 139:227–240. https://doi.org/10.1016/j.revpalbo.2005.07.008

Piçarra JM, Le Meen J (1994) Ocorrência de crinóides em mármores do Complexo Vulcano-Sedimentar Carbonatado de Estremoz: implicações estratigráficas. Comun Inst Geol Mineiro 80:15–25

Piçarra JM, Sarmiento G (2006) Problemas de posicionamento estratigráfico dos Calcários Paleozóicos da Zona de Ossa Morena (Portugal). In: Mirão J, Balbino A (eds) VII Congresso Nacional de Geologia abstract book, vol II. Estremoz, pp 657–660

Pin C, Fonseca PE, Paquette J-L, Castro P, Matte P (2008) The ca. 350 Ma Beja igneous complex: a record of transcurrent slab break-off in the Southern Iberia Variscan belt? Tectonophysics 461(1):356–377. https://doi.org/10.1016/j.tecto.2008.06.001

Ribeiro A, Munhá J, Dias R, Mateus A, Pereira E, Ribeiro ML, Fonseca P, Araújo A, Oliveira JT, Romão J, Chaminé HI, Coke C, Pedro J (2007) Geodynamic evolution of the SW Europe Variscides. Tectonics 26:1–24. https://doi.org/10.1029/2006TC002058

Ribeiro A, Munhá J, Fonseca PE, Araújo A, Pedro J, Mateus A, Tassinari C, Machado G, Jesus A (2010) Variscan ophiolite belts in the Ossa-Morena Zone (Southwest Iberia): geological characterization and geodynamic significance. Gondwana Res 17:408–421. https://doi.org/10.1016/j.gr.2009.09.005

Ribeiro ML, Reche J, López-Carmona A, Aguilar C, Bento dos Santos T, Chichorro M, Dias da Silva Í, Díez-Montes A, González-Clavijo E, Gutiérrez-Alonso G, Leal N, Liesa M, Martínez FJ, Mateus A, Mendes MH, Moita P, Pedro J, Quesada C, Santos JF, Solá AR, Valverde-Vaquero P (2019) Variscan metamorphism. In: Quesada C, Oliveira JT (eds) The geology of Iberia: a geodynamic approach. Vol.2: the Variscan cycle, Regional Geology Series. Springer, Berlin, pp 431–495. https://doi.org/10.1007/978-3-030-10519-8_12

Rossman GR, Aines RD (1991) The hydrous components in garnets: grossular-hydrogrossular. Am Min 76:1153–1164

Robardet M, Gutiérrez-Marco JC (2004) The Ordovician, Silurian and Devonian sedimentary rocks of the Ossa-Morena Zone (SW Iberian Peninsula, Spain). J Iber Geol 30:73–92

Rollinson HR, Pease V (2021) Using geochemical data: to understand geological processes. Cambridge University Press, pp 660 https://doi.org/10.1017/9781108777834

Salman K (2004) The timing of the Cadomian and Variscan cycles in the Ossa-Morena Zone, SW Iberia: granitic magmatism from subduction to extension. J Ib Geol 30:119–132

Sánchez-García T, Bellido F, Quesada C (2003) Geodynamic setting and geochemical signatures of Cambrian-Ordovician rift-related igneous rocks (Ossa-Morena Zone, SW Iberia). Tectonophysics 365(1–4):233–255. https://doi.org/10.1016/S0040-1951(03)00024-6

Sánchez-García T, Quesada C, Bellido F, Dunning GR, Tánago JG (2008) Two-step magma flooding of the upper crust during rifting: the Early Paleozoic of the Ossa Morena Zone (SW Iberia). Tectonophysics 461(1–4):72–90. https://doi.org/10.1016/j.tecto.2008.03.006

Sánchez-García T, Bellido F, Pereira MF, Chichorro M, Quesada C, Pin C, Silva JB (2010) Rift-related volcanism predating the birth of the Rheic Ocean (Ossa-Morena zone, SW Iberia). Gondwana Res 17(2):392–407. https://doi.org/10.1016/j.gr.2009.10.005

Sánchez-García T, Pereira MF, Bellido F, Chichorro M, Silva JB, Valverde-Vaquero P, Pin C, Solá AR (2014) Early Cambrian granitoids of North Gondwana margin in the transition from a convergent setting to intra-continental rifting (Ossa-Morena Zone, SW Iberia). Int J Earth Sci 103:1203–1218. https://doi.org/10.1007/s00531-013-0939-8

Sánchez-García T, Chichorro M, Solá AR, Álvaro JJ, Díez-Montes A, Bellido F, Ribeiro ML, Quesada C, Lopes JC, Dias da Silva Í, González-Clavijo E, Gómez Barreiro J, López-Carmona A (2019) The Cambrian-Early Ordovician Rift Stage in the Gondwanan units of the Iberian Massif. In: Quesada C, Oliveira JT (eds) The geology of Iberia: a geodynamic approach. Vol.2: the Variscan cycle, Regional Geology Series. Springer, Berlin, pp 27–74. https://doi.org/10.1007/978-3-030-10519-8_2

Sarrionandia F, Sánchez MC, Eguiluz L, Ábalos B, Rodríguez J, Pin C, Ibarguchi JG (2012) Cambrian rift-related magmatism in the Ossa-Morena Zone (Iberian Massif): geochemical and geophysical evidence of Gondwana break-up. Tectonophysics 570:135–150. https://doi.org/10.1016/j.tecto.2012.07.023

Sarmiento GN, Gutiérrez-Marco JC, Del Moral B (2008) Conodontos de la "Caliza de Pelmatozoos" (Ordovícico Superior), Norte de Sevilla, Zona de Ossa-Morena (España). Coloquios De Paleontol 58:73–99

Sarmiento GN, Gutiérrez-Marco JC, Rodríguez-Cañero R, Martín Algarra A, Navas-Parejo P (2011) A brief summary of Ordovician Conodont Faunas from the Iberian Peninsula. In: Gutiérrez-Marco JC, Rábano I, García-Bellido D (eds) Ordovician of the world. Cuadernos del Museo Geominero IGME, vol 14, pp 505–514

Santos JF, Soares de Andrade A, Munhá JM (1990) Magmatismo Orogénico Varisco no Limite Meridional da Zona de Ossa-Morena. Comun Serv Geol Portugal 76:91–124

Sharma RS, Sharma A (2020) Metamorphism of dolomites and limestones. Encyclopedia of geology, 2nd edn, pp 479–491. https://doi.org/10.1016/B978-0-08-102908-4.00133-8

Silva JC, Mata J, Moreira N, Fonseca PE, Jorge RCGS, Machado G (2011) Evidence for a lower Devonian subduction zone in the southeastern boundary of the Ossa-Morena-Zone. VIII Congresso Ibérico de Geoquímica (abstract book), Castelo Branco, Portugal, pp 295–299

Silvério G, Pereira S, Moreira N, Piçarra J, Machado G (2021) Tentaculites e cornulitídeos de Portugal: revisão bibliográfica e museológica. Com Geol 108(I):153–158. https://doi.org/10.34637/83v6-xw38

Simancas F, Expósito I, Azor A, Martínez Poyatos D, González Lodeiro F (2004) From the Cadomian orogenesis to the Early Palaeozoic Variscan rifting in Southwest Iberia. J Iber Geol 30:53–71

Solís-Alulima B, López-Carmona A, Abati J (2020) Ordovician metamorphism and magmatism preserved in the Ossa Morena Complex: SHRIMP geochronology, geochemistry and SrNd isotopic signatures of the Sierra Albarrana Domain (SW Iberian Massif). Lithos 374:105700. https://doi.org/10.1016/j.lithos.2020.105700

Solís-Alulima B, López-Carmona A, Abati J, Rojas-Agramonte Y, Bousquet R, del Tánago JG (2023) Polycyclic metamorphic evolution of the Sierra Albarrana Schists (SW Iberian Massif): from low-pressure Ordovician rifting to medium-pressure Variscan overprint. Lithos 444:107092. https://doi.org/10.1016/j.lithos.2023.107092

Veizer J, Ala D, Azmy K, Bruckschen P, Buhl D, Bruhn F, Carden GAF, Diener A, Ebneth S, Godderis Y, Jasper T, Korte C, Pawellek F, Podlaha OG, Strauss H (1999) 87Sr/86Sr, δ13C and δ18O evolution of phanerozoic seawater. Chem Geol 161:59–88. https://doi.org/10.1016/S0009-2541(99)00081-9

Winkler HGF (1976) Petrogenesis of metamorphic rocks. Springer, p 334

Winter JD (2014) Principles of igneous and metamorphic petrology, vol 2. Pearson education, Harlow, p 738. ISBN 10:1-292-02153-5

Winter JD (2020) Metamorphic grades, zones, facies and facies series. Encyclopedia of geology, 2nd edn, pp 439–444. https://doi.org/10.1016/B978-0-08-102908-4.00034-5